Complement receptor *C3ar1* deficiency does not alter brain structure or functional connectivity across early life development

Hanna Lemmik[1], Eugene Kim[1], Eilidh MacNicol[1], Davide Maselli[2], Michel Bernanos[1], Zhuoni Li[3], Dauda Abdullahi[1,4], Esther Walters[1], Maria Elisa Serrano Navacerrada[1], Wuding Zhou[5], Aleksandar Ivetic[2], Diana Cash[1†], Laura Westacott[6†]

[1]Department of Neuroimaging, King's College London, London, UK [2]School of Cardiovascular and Metabolic Medicine & Sciences, King's College London, London, UK [3]Department of Forensic and Neurodevelopmental Sciences, King's College London, London, UK [4]Department of Human Anatomy, College of Medical Sciences, Abubakar Tafawa Balewa University, Bauchi, Nigeria [5]Peter Gorer Department of Immunobiology, King's College London, London, UK [6]Neuroscience and Mental Health Innovation Institute, Cardiff University, Cardiff, UK

†Diana Cash and Laura Westacott contributed equally to this work.

Correspondence: Hanna Lemmik, hanna.lemmik@kcl.ac.uk
Centre for Biomarker Research and Imaging for Neuroscience
Department of Neuroimaging
Institute of Psychiatry, Psychology & Neuroscience
King's College London
James Black Centre (1st floor), 125 Coldharbour Lane, London, SE5 9NU, UK

Abstract

Genetic deletion of the complement C3a anaphylatoxin chemotactic receptor (*C3ar1*), a key component of the innate immune response, is reported to induce behavioural phenotypes resembling anxiety and hyperactivity in mice, suggesting a neurodevelopmental role for this gene in health. However, it is not currently clear when and where *C3ar1* is needed in the brain, which is further complicated by the fact that *C3ar1* is expressed predominantly by microglia and therefore does not localise to specific brain regions, warranting exploratory and brain-wide assessment through neuroimaging. Resolving when and where *C3ar1* is needed are questions of significant translational importance because, as a G-protein-coupled receptor, human C3AR1 serves as a potential therapeutic target for disorders associated with complement upregulation, such as schizophrenia. To provide a brain-wide assessment of developmental *C3ar1* activity, we used longitudinal MRI in male and female adolescent and adult mice ($N = 34$ *C3ar1^{tm1Cge/tm1Cge}* and $N = 35$ *C3ar1^{+/+}*) to estimate regional brain volume using tensor based morphometry, white matter microstructure using fractional anisotropy from diffusion-weighted MRI, and functional connectivity from blood oxygen-level dependent MRI, with behavioural assessment in adulthood. We repeated structural MRI measures in this cohort *ex vivo* to achieve higher resolution. We further repeated *in vivo* structural assessment preceded by behavioural testing in adulthood in a second cohort of mice ($N = 20$ *C3ar1^{tm1Cge/tm1Cge}* and $N = 19$ *C3ar1^{+/+}*) to improve confidence in our findings. We achieved low regional brain volume variability,

allowing us to resolve previously reported sexually dimorphic effects. We were further able to confirm a well-known developmental increase in fractional anisotropy. Despite being able to detect these established effects, we did not find a robust *C3ar1*-dependent phenotype in any of the measures we tested, including behaviour, which may be attributed to our study being the first behavioural study in *C3ar1*-deficient mice to include littermate controls. Therefore, our data do not support neurodevelopmental hypotheses for *C3ar1*, which is encouraging for therapeutic strategies targeting this receptor since interventions are unlikely to disrupt brain development.

Short title: Brain structure and function of *C3ar1* KOs

Key words: C3aR1, behaviour, tensor-based morphometry, fractional anisotropy, BOLD fMRI

Introduction

The complement system is a conserved immune pathway that participates in host defence through pathogen clearance and regulating inflammation[1] as well as tissue homeostasis,[2,3] with emerging roles in neurodevelopment, psychiatric disorders and neurodegeneration.[4–6]

The most convincing evidence for the involvement of the complement system in neurodevelopment so far is its genetic association with schizophrenia. Schizophrenia is a complex and highly heritable neurodevelopmental disorder characterised by hallucinations, delusions, and impaired cognition, with symptoms typically emerging in late adolescence or early adulthood.[7,8] Neurobiological hallmarks of schizophrenia include grey matter loss[9] and a reduction in synaptic density.[10] Genome-wide association studies (GWAS) of schizophrenia have helped to identify two complement-related risk loci; a structural variant in the complement component 4 A (*C4A*) gene,[6] which encodes the C4A protein responsible for propagation of complement activation, and a variant in the CUB and Sushi Multiple Domains 1 (*CMSD1*) gene, which encodes a putative complement inhibitor protein.[11,12] Preclinical studies link these variants to increased brain-specific complement activation and synapse loss,[6,12,13] potentially tying complement activation to synaptic pathology in schizophrenia. Indeed, the *C4A* schizophrenia-risk genotype associates with MRI markers of grey matter loss and reduced cognitive performance in humans, even in the absence of neurological disorders.[14] Further, patients with elevated complement proteins have more severe negative symptoms in psychosis,[15] which typically do not respond to anti-psychotic medication. Complement modulation therefore has potential in addressing this unmet therapeutic need.

C3a anaphylatoxin chemotactic receptor (C3aR1), a G-protein coupled receptor (GPCR) bound by complement activation product C3a and the granin family neuropeptide TLQP-21,[16] acts downstream of complement activation and stands out as a pharmacologically tractable target for modifying complement activity in the brain.[17] In the brain, *C3ar1* transcripts are predominantly expressed by microglia according to Allen Brain Map Transcriptomic explorer mouse and human data (microglia markers *Itgam*, *Cx3cr1* and *C1qb*) and Stevens lab microglia single cell atlas (sorted by FACS; *Cd45^{low}*, *Cd11b^{high}*, *Cx3cr1^{high}*), with minimal neuronal expression.[18,19] While its temporal expression patterns are not yet well characterised, C3aR1 appears to be active

2

during early embryonic development, potentially influencing progenitor cell proliferation.[18,20,21] C3aR1 also appears to facilitate developmental astrocyte phagocytosis by microglia in the retina,[22] as well as to regulate microglial reactivity and neuroinflammation more broadly.[23–28] Brain morphological changes observed in *C3ar1*-deficient mice further support its neurodevelopmental relevance,[29,30] although there is no consensus on the precise neurodevelopmental actions of C3aR1. Addressing this gap is important given this receptor's potential as a pharmacological target.

C3aR1 signalling may impact brain functions relevant to psychiatric symptomatology since a range of behavioural phenotypes have been reported in *C3ar1*-deficienct mice. These include abnormal anxiety-like behaviours,[31] hyperactivity,[30] cognitive impairment[20] but also a resilience to depressive-like behaviours induced by chronic stress or inflammation.[32–34] Although the observed involvement of C3aR1 in adult behaviour suggests that it is needed for normal brain function, previous studies have not addressed the question of whether these phenotypes arise because of a C3aR1 deficit during development or because it is continuously needed, which can be resolved through longitudinal assessment. Another important yet overlooked aspect is the use of the appropriate wild-type *littermate* control animals that none of the aforementioned studies included. Instead, these studies used separately raised cohorts of control and mutant mice which represents a known confound due to the rapidly diverging genetic backgrounds in small inbred colonies,[35] but also because litter environment affects behaviour and brain development.[36–38]

To investigate the potential consequences of *C3ar1* deficiency during development, we adopted a global, unbiased approach, conducting a longitudinal study of male and female *C3ar1*-deficient mice and their wild-type littermates during adolescence (postnatal day, PND27–31) and adulthood (PND81–92). Using structural and diffusion magnetic resonance imaging (MRI and dMRI), as well as resting state fMRI (rsfMRI), we aimed to assess whether the absence of C3aR1 affects brain development during adolescence—a critical period for psychiatric vulnerability[39,40]—or whether this requirement only becomes evident by adulthood.

Our imaging measures included regional brain volumes derived from tensor-based morphometry (TBM), fractional anisotropy (FA) from dMRI to evaluate white matter organisation, which is influenced by microglial activity during development,[41,42] and graph theoretical analysis of functional connectivity (FC) correlates of blood oxygenation level dependent (BOLD) signal, such as global efficiency and clustering coefficient to characterise brain network topology.[43–45] These techniques were complemented by behavioural testing in adult mice that measured cognition and emotional reactivity, as we sought to replicate previously reported behavioural experiments in *C3ar1*-deficient mice.[20,30,31] Unexpectedly, we found no robust brain or behavioural phenotype in our datasets, challenging the previous assumptions of a neurodevelopmental role for C3aR1 under physiological conditions.

3

Methods and materials

Animals

All animal procedures complied with the UK Animals and Scientific Procedures Act 1986 and were approved by the local ethical committee at King's College London (KCL). Homozygous *C3ar1$^{tm1Cge/tm1Cge}$* mice were generated by homologous recombination in embryonic stem cells and kindly provided by Dr. Bao Lu and Prof. Craig Gerard (Harvard Medical School, Boston, MA).[46] These mice were subsequently backcrossed onto the C57BL/6J strain for at least 12 generations and maintained on a C57BL/6J background in Professor Wuding Zhou's laboratory in KCL. For this study, cryopreserved stocks were rederived in KCL and crossed to C57BL/6J mice purchased from Charles River to refresh the genetic background following Jackson's Laboratories line refreshing protocol. **See Supplemental methods for further notes on experimental animals**.

Validation of mutation

Bone marrow-derived macrophages were obtained from tibias and femurs of eight three-month-old mice (*N* = 4 *C3ar1$^{+/+}$, N* = 4 *C3ar1$^{tm1Cge/tm1Cge}$*). Bone marrow suspension was filtered through a 40 μm mesh, centrifuged at 450 x g for 5 minutes at 4°C, and treated with NH_4Cl haemolysis buffer (NH_4Cl 0.15M, $KHCO_3$ 0.01M, EDTA 0.0001M). After a second centrifugation under the same conditions, cells were washed with PBS and resuspended in Gibco RPMI 1640 Medium (Thermo Fisher, #21875-034) supplemented with 50 ng/ml recombinant mouse macrophage colony-stimulating factor (M-CSF, R&D Systems, #416-ML-010/CF), 1% penicillin, 1% streptomycin, and 10% heat-inactivated foetal bovine serum (Sigma, #F9665-50ml).

Cells were seeded at $1x10^6$ cells/ml in six-well plates (six wells per animal) and incubated at 37°C with 5% CO_2 for 72 hours. On day three, the medium was refreshed, and 50 ng/ml recombinant mouse IL4 (R&D Systems, #404-ML-010/CF) was added to half of the wells to skew them towards M2 phenotype. Incubation continued for an additional 48–72 hours, depending on cell confluence.

RNA extraction, cDNA synthesis, gel electrophoresis and qPCR were conducted using standard protocols, details of which can be found in the **Supplementary methods**.

Study design

This study used two separate cohorts of male and female *C3ar1*-deficient *C3ar1$^{tm1Cge/tm1Cge}$* and littermate wild-type mice. The main, longitudinal MRI cohort (*N* = 35 *C3ar1$^{+/+}$, N* = 34 *C3ar1$^{tm1Cge/tm1Cge}$*, *N* = 20 litters), termed Cohort 1, had *in vivo* MRI performed in adolescence (range 27–31 days) and adulthood (range 81–92 days), and the adulthood MRI scan was preceded by the open field (OF) and elevated plus maze (EPM) tests. The adolescence time-point was chosen because mice reach puberty approximately between PND24–34.[47–49] Synaptic remodelling occurs in two waves in mice and humans—during early perinatal development and in adolescence.[39] By including a pre-pubertal timepoint, we aimed to determine whether changes occur during the initial wave of pruning or emerge specifically between adolescence and adulthood. Behavioural testing was limited to adult animals, as aberrant behavioural phenotypes in *C3ar1* knockouts have only been reported during adulthood to date. *Ex*

4

vivo imaging was conducted in Cohort 1's perfusion-fixed brains after the final adulthood scan.

For Cohort 2 (N = 19 *C3ar1*$^{+/+}$, N = 20 *C3ar1*$^{tm1Cge/tm1Cge}$, N = 13 litters), behavioural testing was conducted similarly to Cohort 1 in adulthood only (range 74–110), and consisted of OF, novel object recognition (NOR), EPM and prepulse inhibition (PPI) tests followed by *in vivo* structural and diffusion MRI (note that MRI was not conducted in adolescence in this cohort). For both cohorts, behavioural testing was conducted 2–7 days before the adulthood scan. **See Supplemental methods for behavioural experiment details and Supplemental figure 1 for genotype and sex ratios of experimental animals**.

The sample size of Cohort 1 was statistically powered to detect medium effect sizes in regional volume using TBM across four groups (males and females analysed separately), with a minimum sample size of N = 15 per group based on previously observed variance with this method by our group.[50] Cohort 2 sample size was powered to detect medium effect sizes in regional TBM with sexes combined, N = 16 per group.

In vivo MRI

Two to three days after behavioural testing, mice were imaged using a Bruker BioSpec 9.4 T scanner with an 86-mm volume resonator for transmission and a 4-channel surface array coil. Anaesthesia was induced with 4% isoflurane in medical air (1 L/min) and oxygen (0.4 L/min), maintained at 2% but adjusted based on respiration rates. For BOLD fMRI in Cohort 1, we used a medetomidine and isoflurane anaesthesia optimised for mouse fMRI.[51] This consisted of a subcutaneous medetomidine bolus (0.05 mg/kg) followed ten minutes later by its continuous infusion (0.1 mg/kg/h), with isoflurane levels gradually reduced to 0.45-0.65% over 15 minutes from the start of the infusion. BOLD fMRI was conducted after the structural scans, which took a further 45-60 minutes after reducing isoflurane level. The respiration rate was monitored with a pressure sensor, and temperature was monitored with a rectal thermometer and maintained at 36–37°C using a water circulation system. **For image pre-processing and further MRI details, see Supplemental methods**.

Study templates

The `antsMultivariateTemplateConstruction2.sh` script from ANTs was used to create study specific templates from processed images. For *in vivo* scans of Cohort 1, magnetisation transfer weighted (MTw), T1w, R2* map (generated from the multi-gradient-echo proton density weighted, T1w and MTw images using the `qi mpm_r2s` command in the QUIT package), S0, fractional anisotropy (FA) and mean diffusivity (MD) images were used. For the *ex vivo* scans of Cohort 1, separate T2w and diffusion weighted images (DWI) templates were created comprising S0 which is an estimated non-diffusion-weighted image from `dtifit`, FA, and MD images. For Cohort 2, PDw, T1w, MTw, S0, FA, and MD images were used. For BOLD fMRI, the study template was a T2w image derived from a separate mouse study conducted at the BRAIN Centre (KCL). The use of this external template was justified by the low resolution of fMRI, which does not benefit from creating a study-specific template.

5

Jacobian determinant maps

To estimate volume, Jacobian determinant maps were generated from the deformation fields corresponding to the transformation of each subject to the study template using the `CreateJacobianDeterminantImage` command from ANTs. The Jacobian determinant values of all voxels within the template brain mask were summed to obtain the total brain volume of each subject. Jacobian determinants were calculated from the combined rigid, affine, and Symmetric Normalization (SyN) transforms as well as from only the SyN transforms to obtain maps of absolute and relative volume (accounting for differences in global brain volume), respectively. For TBM, the Jacobian determinants were subsequently log-transformed.

Voxel-wise analysis

For voxel-wise statistics, FSL randomise with permutation testing was used (10,000 for Cohort 1, 5000 iterations for Cohort 2) followed by a threshold-free cluster enhancement (TFCE) and family-wise error (FWE) correction as described in.[52,53] Given the absence of genotype differences in total brain volume, TBM regional volumes are reported relative to total brain size for greater accuracy.[54] For sex differences, absolute volume maps are reported in the Supplemental material.

Common coordinate space

The study template was registered to the Allen Mouse Brain Common Coordinate Framework[55] using ANTs, and the Allen atlas was subsequently transformed to the study template space with the inverse transform.

ROI-based analysis of volume

The images were segmented using an in-house modified version of the Allen atlas of 72 regions.[50,55] These segmentations were subsequently used to compute regional volumes by summing the Jacobian determinants within each parcellation.

Regional volume variability was estimated by calculating a coefficient of variation (CV) for each region with normalised root-mean-square method for each genotype in each experiment, using the calculation: $CV = \frac{\sigma}{\mu}$, where σ is the standard deviation and μ the population mean for each region in the atlas ($N = 72$ regions). Group differences in CV were calculated with a Kruskal-Wallis test (SciPy.stats, `kruskal`).

Fractional anisotropy

For mass-univariate voxel-wise analysis of fractional anisotropy, values from `dtifit` for Cohort 1 were again analysed with FSL randomise with permutation testing (10,000 permutations) followed by TFCE and FWE-correction. FA is not reported for Cohort 2 in this manuscript for brevity (null results). For ROI-based analysis, voxel FA medians within parcellation were used for all white matter regions.

To calculate the change over time in fractional anisotropy in the longitudinal study, adolescence values for each voxel value or regional median were subtracted from adulthood values. Differences between genotypes were calculated with a mixed ANOVA with between-subjects factor of genotype and within-subjects factor of region.

6

Change from 0 was calculated with a two-sided one-sample *t* test (SciPy.stats, `ttest_1samp`), which was corrected with the Benjamini–Hochberg (BH) method.

Functional connectivity and graph theory analysis

For functional analysis, a high-level parcellation scheme was applied to segment 36 unilateral regions (18 per hemisphere) excluding white matter from the acquired 3D volume. The BOLD signal time-courses were averaged within each ROI, and the mean time-courses were extracted using FSL's `fslmeants` tool. Pearson correlation coefficients were calculated for each time-course pair, producing a 36×36 correlation matrix for each subject. These matrices were analysed as functional connectivity (FC) graphs, with edge strength determined by the Fisher z transformed Pearson correlation coefficient. To identify the strongest connections, graphs were thresholded at 5% intervals from 5% to 50%. At each threshold level, referred to as the graph sparsity interval, connections below threshold were set to zero, generating 10 sparsity graphs per subject. FC was calculated as the average non-zero connectivity at each threshold level. Global graph metrics, global efficiency and clustering coefficient, were computed at each sparsity level using Brain Connectivity Toolbox algorithms[56] implemented with Network X (3.4.2) `global_efficiency` and `clustering` passing thresholded Pearson matrices. The area under the curve (AUC) was computed per subject using trapezoidal numerical integration (`numpy.trapz`), and the likelihood of observed values was estimated with permutation testing (10,000 permutations).

To estimate changes over time, global graph metric values at adolescence were subtracted from adulthood values at each sparsity interval. Group differences were again tested by calculating the AUC and applying permutation testing. Changes from baseline (zero) were evaluated using two-sided one-sample *t* tests (difference from 0), corrected for multiple comparisons with the BH method.

FDR correction and network-based statistics

Matrices for *C3ar1*-deficient and wild-type mice were compared with Student's *t* tests for each pairwise connection, resulting in 36×36 *t*-statistic and *p*-value matrices. To control for multiple comparisons, FDR correction was applied to the upper triangle of the *p*-value matrix using the BH procedure.

For network-based statistics (NBS), the above-described *t* matrices were thresholded at $|t| \geq 2$. To identify connected components within the FC graph, adjacency matrices representing significant connections ($|t| \geq 2$) were converted into graph objects using NetworkX. Regions of interest (ROIs) were treated as nodes, and significant connections as edges. Connected components were identified using a breadth-first search (BFS) algorithm, which explores all neighbouring nodes before moving deeper into the graph. Only components containing more than one ROI were retained for further analysis. To generate a null distribution of maximal component sizes, group labels were randomly shuffled across subjects for each permutation while preserving matrix structure (10000 permutation). The *p*-value for an observed component was calculated as the proportion of permutations where the maximal component size exceeded that of the observed component.

7

A priori node strength analysis

We selected 20 (10 left +10 right) anxiety and fear related regions (cingulate cortex, prefrontal cortex, amygdala, pallidum and nucleus accumbens, striatum, hypothalamus, dorsal hippocampus, ventral hippocampus, periaqueductal grey, brain stem) and calculated their average absolute connectivity to all other regions using Fisher z-transformed Pearson correlation coefficients. We then used a mixed ANOVA with between-subjects factor of genotype and within-subjects factor of region followed by pairwise testing with BH method.

Within-network analysis

Two mouse resting state networks were subset from correlation matrices: the default mode network (DMN) and the salience network.[57,58] The DMN included bilateral prefrontal cortex, cingulate cortex, and dorsal hippocampus, while the salience network comprised bilateral cingulate cortex, amygdala, and striatum. Additionally, a third anxiety-related network was defined, consisting of the 20 regions described in the node-strength analysis above.

For each network, mean FC was calculated as the average of all pairwise connections between nodes within the network, without applying a threshold. For individual network global efficiency analysis, thresholding was not used due to the small number of nodes. Instead, Pearson matrices normalised to range from 0–1 were passed to bctpy (0.6.1) `efficiency_wei` computing weighted efficiency.

Student's *t* tests were used to test significance, and the comparisons were corrected within outcome measure with the BH method.

Voxel-wise seed-to-brain analysis

We conducted voxel-wise seed-based FC analyses for anxiety-related regions, as well as the colliculus and sensory cortex, which served as control regions not specific to anxiety. For each seed region, the time-course of the BOLD signal was extracted and regressed with the BOLD signal of every voxel in the brain, resulting in a 3D spatial map of the connectivity with the seed. Group-level comparisons of these maps were performed between genotypes using voxel-wise permutation tests with FSL's randomise (5000 permutation), converted with TFCE and statistical significance corrected for multiple comparisons using FWE (seed-to-brain), but these were not corrected for the presence of multiple seeds.

Statistical procedure for behavioural outcome measures

All statistical analyses were conducted using Python 3.11.7, using relevant libraries such as SciPy and statsmodels. For both studies, the Shapiro-Wilk test was used to assess the normality of data distributions, while Levene's test was used to evaluate homogeneity of variances. When either assumption of normality or equal variance was violated, the Kruskal-Wallis test was used, followed by Dunn's test for post hoc pairwise comparisons with Bonferroni correction for multiple testing where applicable. For datasets meeting parametric assumptions, different approaches were used based on the study design. For Cohort 1, a two-way ANOVA was performed to analyse the effect of sex, genotype and sex-by-genotype interaction, followed by Tukey's test for post hoc comparisons. Bonferroni correction was applied to adjust for multiple comparisons. Due

8

to the relatively small sample size ($N = 38$) in Cohort 2, sex-by-genotype interactions were not analysed. Instead, Student's t tests were used for comparisons between groups.

To balance statistical rigor with preserving power in exploratory contexts, behavioural measures were not universally corrected for multiplicity. Instead, robustness was inferred through replication across independent cohorts and broad phenotypic consistency. The threshold for statistical significance was set at $p < 0.05$. Individual mice served as the experimental units in all analyses.

Results

C3ar1^{tm1Cge/tm1Cge} mice lack detectable *C3ar1* mRNA

We used an established *C3ar1* mutant line, *C3ar1*^{tm1Cge},[46] and performed our own validation of the mutation. For this purpose, we designed a 79-base pair (bp) amplicon targeting the putatively deleted region (**Figure 1A**). PCR analysis of cDNA derived from bone marrow-derived macrophages—a cell type consistently reported to express high levels of *C3ar1* mRNA[59–61]—showed no detectable transcript in this region in the mutant animals (**Figure 1C**), confirming the absence of the canonical transcript. The *C3ar1* gene contains an in-frame start codon after the deletion (**Supplemental figure 2**). We also confirmed that no transcript is made that includes this region (**Figure 1B**). These results were further corroborated by quantitative PCR (qPCR, $N = 8$) in homozygous knockout animals in either M0-like (**Figure 1D**) or interleukin 4 (IL4)-induced M2-like macrophages (**Figure 1E**, see **Supplemental figures 3C–E** for macrophage polarisation confirmation). Together, these results confirm that *C3ar1*^{tm1Cge} is a true loss-of-function or a "knockout" allele resulting in no detectable *C3ar1* transcript.

C3ar1-deficiency does not influence total or regional brain volume

We conducted a longitudinal MRI study (referred to as Cohort 1 hereafter or implied when cohort is not specified) to investigate potential genotype-related differences in brain structure and function using *C3ar1*^{tm1Cge/tm1Cge} homozygous knockout mice (also referred to as *C3ar1*-deficient) and their littermate wild-type controls (*C3ar1*^{+/+}) (**Figure 2A**) on C57BL6J (Charles River, UK) background. Both groups underwent *in vivo* MRI in adolescence (PND27–31) and adulthood (PND81–92). Structural MR images were additionally collected *ex vivo* from the same mice sacrificed in adulthood immediately after the *in vivo* scan to achieve higher isotropic resolution (0.1 mm *ex vivo* vs 0.15 mm *in vivo*) and increased signal-to-noise ratio (SNR). To corroborate these results, we also conducted MRI in adulthood (PND74-110) in an independent study cohort, referred to as Cohort 2.

We used tensor-based morphometry (TBM) analysis to estimate total brain volume and to map regional brain volume differences. There were no genotype-dependent differences in total brain volume *in vivo* in adolescence (**Figure 2B**) nor in adulthood (**Figure 2C**). In all adolescent mice, irrespective of genotype, female mice exhibited significantly smaller total brain volumes compared to males. These sex differences disappeared by adulthood—a finding that aligns with previous observations in wildtype mice.[62]

9

Still using TBM, no significant genotype-dependent differences in regional brain volumes were detected in adolescence (**Figure 2Di**). In adulthood (**Figure 2Dii**), *C3ar1*[tm1Cge/tm1Cge] mice showed a significant (TFCE-corrected $p < 0.05$) volume increase in the right pretectal area (72 voxels), and subthreshold ($0.05 <$ TFCE-corrected $p < 0.5$) increases in the left pretectal area (111 voxels) and the right lateral thalamus *in vivo*, but these differences were no longer observed in the same study cohort *ex vivo* despite improved spatial resolution (not shown since these group-level data would be presented as empty study-template maps), nor did we observe any genotype-dependent differences using TBM analysis in Cohort 2 (not shown). We also did not observe any significant genotype-by-sex interaction effects (not shown).

While no reproducibly significant genotype effects in regional volumes were observed in Cohort 1, we nevertheless detected sexually dimorphic effects (**Figure 2Diii** and **2d-iv**). Adolescent female mice had significantly larger volumes (relative to total brain volume) bilaterally in the agranular insular cortex (AI), superior colliculus (SC), medial septum (MS) and in the CA1 region of the hippocampus, whereas male mice had increased relative volumes in white matter areas including the olfactory tract, corpus callosum, hippocampal commissure, and notably also in the median preoptic nucleus (MEPO) which is well known to be larger in male rodents[63] (**Figure 2Diii, Supplemental figure 4** for absolute volume). Echoing total brain volume measures, many of these sex differences were no longer observed in adulthood (see also **Supplemental figure 5** for Cohort 2 data), but females showed larger relative volumes in the dorsal anterior cingulate cortex (ACAd), secondary motor cortex (MOs) and primary somatosensory cortex (SSp). Adult males had larger relative volumes in areas including the medial amygdala (MEA) and the bed nucleus of stria terminalis (BST) which, like the MEPO, are previously documented sexual dimorphisms[64] and which were also observed *ex vivo* in this study cohort (**Supplemental figure 6**).

There were no genotype nor sex-by-genotype interactions on regional brain volumes at either time-point (not shown). Overall, female somatosensory and motor cortices increased more in volume between adolescence and adulthood than male (**Supplemental figure 7**), in line with the observed smaller differences in these areas in adulthood compared to adolescence.

If variability was high within our study sample, particularly in the *C3ar1*-deficient group, it would have hampered our ability to detect significant differences. The coefficient of variation for grey matter region-of-interest (ROI) volume showed no differences between genotypes *in vivo* in adolescence (**Figure 2E**) or adulthood (**Figure 2F**), nor *ex vivo* in adulthood (**Figure 2G**). The overall variability was low, ranging from 4.2–5.5% *in vivo* and 4.2% *ex vivo*, while hippocampal variability which has previously been repeatedly measured establishing a neuroimaging gold standard at 5% variability,[54] was 3.7–3.8% *in vivo* and 4.2% *ex vivo* in our study. These values suggest that our study was well-positioned to detect a genotype effect if one had been present.

C3ar1-deficiency does not influence fractional anisotropy

To assess the potential impact of *C3ar1* deficiency on white matter integrity, we measured fractional anisotropy (FA) as an indirect marker of axonal microstructure[65] (**Figure 3**). Using voxel-wise analysis, we observed sub-threshold, non-significant ($0.05 < p < 0.5$) decreases in FA in *C3ar1*-deficient mice compared to wild-types (**Figure**

10

3A). In adolescence, sub-threshold reductions were noted in the corpus callosum (CC) and optic tract (OPT, **Figure 3A**, upper panel). In adulthood, they were primarily localised to the CC (**Figure 3A**, bottom panel). These sub-threshold differences were not observed *ex vivo*. Compared to males, female mice had sub-threshold decreases in FA *in vivo* in adulthood in the internal capsule and in the third ventricle (**Supplemental figure 8**), but this was again not observed *ex vivo* (not shown). We did not observe any sex-by-genotype interactions in our FA datasets (not shown).

In our ROI-based FA analysis, we focused on predefined white matter regions, hypothesising that FA alterations would primarily occur in areas containing axonal tracts due to increased microglial phagocytosis in *C3ar1*-deficient mice during development.[22,41,42] In this analysis also, no significant genotype effects were observed in adolescence (**Figure 3Bi**) or adulthood (**Figure 3Bii**). There were no genotype-dependent differences in the change in FA over time, but FA increased between adolescence and adulthood in all white matter areas except the olfactory tract (**Figure 3Biii**), which is in line with the reported early maturation of the olfaction system in mice.[66]

C3ar1-deficiency does not influence global functional brain connectivity

Functional connectivity (FC) changes have been reported for other microglial receptor knockouts, including triggering receptor expressed on myeloid cells 2 (*Trem2*), CX3C motif chemokine receptor 1 (*Cx3cr1*), and complement receptor 3 (*Cr3*).[67–69] Specifically, *Trem2* and *Cx3cr1* knockout mice exhibited impaired synapse elimination in these studies, alongside decreased FC, social behaviour deficits and increased repetitive behaviour.[67,69] In contrast, *Cr3* knockout mice did not show deficits in synapse or axon refinement but showed reduced phagocytosis of perinatal cortical neurons and higher cortical FC.[68] Since *C3ar1*-deficiency appears to cause a deficit of developmental astrocyte phagocytosis, at least in the retina,[22] it is plausible that a similar mechanism could lead to increased cellular phagocytosis also in the brain parenchyma, as seen with *Cr3* knockouts. This may result in a higher number of neurons during early embryonic development, contributing to increased FC. We estimated FC through analysis of BOLD signal time-courses with the assumption that the magnitude of correlation between these time-courses corresponds to the strength of FC. We calculated pairwise correlation coefficients between 36 (18 per hemisphere) grey matter regions. Non-zero correlation values were averaged across proportional progressively decreasing sparsity thresholds to preserve biologically meaningful weak correlations while minimising noise.[70] No genotype-dependent differences in global FC were observed in adolescence (**Figure 4A**), adulthood (**Figure 4D**) or in the change over time (**Figure 4G**).

We applied graph theory to characterise global brain network connectivity across all regions, focusing on two key metrics: clustering coefficient (**Figure 4B**, **E** and **H**) and global efficiency (**Figure 4C**, **F** and **I**), and applying the same strategy for proportional thresholding as for FC. The clustering coefficient reflects the tendency of nodes to form connected local clusters, with higher values indicating the presence of more highly interconnected subnetworks within the brain.[71] Global efficiency refers to the average of shortest paths linking nodes in a network and can be a proxy of information integration abilities since it decreases with cognitive deficit[72,73] and increases with development.[74] Clustering coefficient and global efficiency appeared higher in *C3ar1*-deficient animals

11

at both time-points, but this was not significant (**Supplemental table 1)**. Further, we found no effects of genotype across global connectivity measures when we treated males and females as separate groups (**Table 1**, for *p* values, see **Supplemental table 2**).

Global efficiency and clustering coefficient appeared to increase with brain maturation when genotype groups were combined, but this was only significant when graph sparsity was lower, that is, when 30–50% of the strongest connections were retained, with small effect sizes observed (Cohen's $d = 0.30–0.32$). These findings indicate that while *C3ar1* deficiency did not result in alterations in global network properties under our experimental conditions, developmental changes in global efficiency and clustering coefficient were detectable.

C3ar1-deficiency does not influence functional brain networks

Since *C3ar1*-deficient mice did not show statistically significant changes in global connectivity metrics, we next examined specific networks after conducting *t* tests for each pairwise ROI FC between genotypes. For this we used two hypothesis-free approaches; false discovery rate (FDR) correction to identify strongly differing edges between genotypes, and network-based statistics (NBS)[75] to detect network-level differences while controlling for family-wise error rate. We thresholded the resulting *t*-value matrices at $|t| \geq 2$ for adulthood and adolescence, and their changes over time (adulthood – adolescence; **Figure 5A**). However, no edges remained significant after FDR correction. Then, using NBS which tests the likelihood of detecting a connected component of a specific size, we determined that the network sizes observed after thresholding at $|t| \geq 2$ ($N = 68$ at adolescence, $N = 15$ at adulthood, and $N = 1$ for change) could occur by chance in these datasets.

Given that neither one of the hypothesis-free approaches, FDR correction and NBS, detected any genotype-related differences, we next focused on anxiety-related regions. This decision was motivated by prior evidence of anxiety-like behaviour in *C3ar1*-deficient animals[31] and the inclusion of anxiety-specific tests in our behavioural battery. We calculated the mean FC, or nodal strength, of 20 *a priori* selected brain regions relevant to anxiety. We did not detect effects of genotype (**Figure 5B**), sex (**Table 2**) or genotype-by-region interaction (**Supplemental table 3**).

Next, we examined FC and global efficiency within two resting state networks that have been linked to anxiety and emotionality in humans[76–78] and that have been observed in mice[57,58,79]; the default mode network (DMN) and the salience network (**Figure 5C**). Additionally, we analysed network connectivity within a third, anxiety network (regions in **Figure 5B**). Consistent with our earlier findings, we did not observe genotype-dependent differences in these networks at either time-point.

Significant genotype-related differences were detected only in our voxel-wise seed-to-brain connectivity analysis (**Figure 6**). However, these findings should be interpreted with caution, as the analysis controlled for voxel-wise comparisons within subjects but did not correct for multiple seed tests, which limits the robustness of the results. Nevertheless, some anxiety-related regions—for example, the left prefrontal cortex and left ventral hippocampus (see **Supplemental Figure 9** for the right hemisphere)—showed weak and widespread increases in connectivity in *C3ar1*-deficient animals

12

compared to controls at both time-points. Seed-based analyses also revealed higher functional connectivity across the brain when other anxiety-related regions were used as seeds, being most pronounced during adolescence (**Supplemental figure 10**). However, this effect was not confined to anxiety-related regions or specific networks (**Supplemental figure 11**). Therefore, being non-specific and weak, these findings cannot at this point be clearly distinguished from noise.

C3ar1-deficient mice do not have discernible behavioural phenotypes

Behavioural testing is another way of assessing functional consequences of genetic manipulations with expected neurodevelopmental sequelae.[80] We aimed to evaluate the impact of *C3ar1* deficiency on anxiety-like behaviour, locomotion and recognition memory, which were chosen based on prior reports of abnormalities in *C3ar1*-deficient mice. We used a battery of well-established behavioural tests, including the OF test and EPM for anxiety-like behaviour and locomotion, as well as NOR for recognition memory. We also tested PPI which is a sensorimotor reflex consistently found to be attenuated in schizophrenia[81,82] but which has hitherto not been tested in *C3ar1*-deficient mice.

We performed behavioural testing in both cohorts described in the structural MRI results sections. In Cohort 1 (**Figure 2A**), behavioural testing (EPM, then OF) occurred shortly before the adulthood MRI scan (and two months after adolescence MRI). Behaviour of Cohort 2 was also tested in adulthood (OF, NOR, EPM, PPI, in that order) followed by MRI, except that these mice were not previously scanned under anaesthesia in adolescence. Behavioural data from each cohort were analysed separately to account for differences in study design.

In Cohort 1, no significant genotype effects were observed for anxiety-like behaviours (**Supplemental table 4** for description of anxiety-like metric selection) or locomotor activity. Specifically, there were no differences between genotypes in OF distance travelled (**Figure 7A**), time spent in the centre 70% of the arena (**Figure 7B**), or time in the periphery (**Figure 7C**). Similarly, EPM measures—including time spent in open arms (**Figure 7D**), in the middle (**Figure 7E**), or in closed arms (**Figure 7F**)—showed no genotype differences. All corresponding statistical results are provided in **Supplemental table 5**.To rule out any potential confounding effects from co-housing littermate mutants and wild-types,[83] we also examined whether the number of *C3ar1*-deficient cage-mates influenced wild-type behaviour but found no consistent pattern or evidence of systematic anxiety-like effects in wild-types (**Supplemental figure 12**). To assess multiple measures of anxiety-like behaviour and locomotion along one another (**Figure 7H–I**), we calculated z-scores for each behavioural outcome measure for *C3ar1*-deficient mice relative to wild-type controls (**Table 3** for untransformed means).

In Cohort 2, most anxiety-related and locomotion measures showed no genotype differences (**Supplemental table 6**), except for reduced distance travelled in the centre of the OF arena by *C3ar1*-deficient mice (uncorrected two-sample *t*-test $p < 0.01$, Cohen's $d = 0.92$). However, no genotype effect on distance was detected in the core of the OF arena or in the centre and core of the OF arena in Cohort 1.

The sample size ($N = 38$) of Cohort 2 was too small to reliably test for interactions between sex and genotype, meaning we only had enough statistical power to detect very

13

large effects (Cohen's $f = 0.5$ at alpha = 0.05 and 80% power), which were clearly not observed across behavioural measures. No sex-by-genotype interactions were observed in Cohort 1 (**Supplemental table 5**).

Additionally, PPI testing (performed exclusively on Cohort 2) showed no effect of *C3ar1* deletion, though PPI increased with prepulse intensity as expected (**Figure 7G**), confirming that the test was set up to reliably measure this phenomenon. NOR testing (also performed exclusively on Cohort 2) revealed no genotype differences, with all groups demonstrating successful learning based on recognition indices significantly above chance levels (**Figure 7J**).

Overall, these findings suggest that *C3ar1* deficiency does not result in robust anxiety-like or hyperactive phenotypes, nor deficits in recognition memory or PPI.

Discussion

Here we used longitudinal neuroimaging and behavioural testing to investigate the impacts of *C3ar1* deletion on brain structure and function across early life development in mice. We found no robust evidence that *C3ar1* deficiency affects total or regional brain volume, white matter FA, global FC, global efficiency, clustering coefficient, or specific functional networks.

We also found no altered behavioural phenotype in either male or female *C3ar1*-deficient mice in adulthood. These results raise questions regarding the source of discrepancies between these data, our previous behavioural work[29,31] and that of others,[20,30,32,34] which may be attributed to our use of littermate controls in this study, as will be elaborated upon in the following sections. Overall, the lack of a behavioural phenotype combined with the lack of genotype effects on brain structure across modalities and time-points means that the role of C3aR1 in neural development and behaviour is likely context dependent.

Absence of *C3ar1*-dependent effects on brain structure

Our morphometric analysis showed that total and regional brain volumes were not changed between *C3ar1*-deficient and wild-type mice. We were, however, able to detect sex-specific neurodevelopmental changes that have previously been reported in rodents, such as brain growth occurring later in females, minimal total and regional brain volume differences in adulthood and larger volume of MEPO and BNST in males,[62–64,84,85], supporting the sensitivity of our methodology. Together with the low variability in our sample, our ability to detect these known sex differences means that we were well-positioned to identify potential genotype effects had they been present. These findings are also consistent with another recent longitudinal MRI study in *C3ar1* knockout mice, which reported no differences in neocortex or hippocampus volumes at three months of age.[86]

Absence of *C3ar1*-dependent effects on white matter fractional anisotropy

In the brain, *C3ar1* is predominantly expressed by microglia,[87,88] where it may influence their reactivity and phagocytosis.[22,23,25–27] Notably, changes in microglial characteristics have been linked to developmental alterations in FA in both mice and humans.[41,42] We found no *C3ar1*-dependent changes in the white matter despite showing the overall

14

effect of time on FA, which is known to increase during development between adolescence and adulthood in both humans and mice.[89–93] Lack of a phenotype after the deletion of a predominantly microglial gene may not be surprising since mice that completely lack microglia for their entire lifespan (achieved by deleting the super enhancer for macrophage colony-stimulating factor receptor, *Csf1r*) do not have overt neurodevelopmental phenotypes,[94] and only show vulnerability in a pathological context involving neuroinflammation.[95] This raises the possibility worth discussing that neurodevelopmental phenotypes associated with *C3ar1* deficiency may likewise only become apparent under neuroinflammatory conditions. There is, however, an important distinction to be made here between an immune trigger during development and an inflammatory stimulus in adult animals. A growing body of literature suggests that *C3ar1* deficiency tends to be mildly anti-inflammatory and protective in contexts such as chronic stress or other neuroinflammatory conditions[23,32,34]—a profile that opposes the proposed hypothesis that *C3ar1* deficiency leads to aberrant phenotypes when combined with an inflammatory insult. Additionally, it is apparently important to distinguish between chronic and acute inflammatory stimuli. For instance, a recent study using scRNA-Seq data from the hippocampus of *C3ar1*-deficient mice given an acute lipopolysaccharide challenge (1 mg/kg i.p.) found that astrocyte, microglia, and oligodendrocyte activation signatures were completely *C3ar1*-independent,[86] indicating that an acute systemic stimulus may be insufficient to reveal a requirement for *C3ar1* in the brain.

With this in mind, it is difficult to support a scenario in which the presence of *C3ar1* is beneficial during development but only under neuroinflammatory conditions, given that available data suggest it has either the opposite effect or no effect in adulthood, and there are currently no littermate-controlled studies to substantiate this developmental hypothesis. However, our study cannot definitively exclude this possibility. Future studies could address this question by incorporating maternal immune activation models or by testing *C3ar1*-deficiency in sensitised backgrounds, such as in the presence of *C4A* overexpression—a known genetic risk factor for schizophrenia[6] that also affects white matter integrity.[96]

Functional connectivity appears *C3ar1*-independent

We did not detect genotype-dependent global FC changes nor changes to clustering coefficient and global efficiency at either time-point. We did, however, observe a genotype-independent developmental increase in global efficiency and clustering coefficient with time, which has been reported before[74,90,97] particularly at lower sparsities,[98] suggesting that our method was sensitive enough to pick up developmentally relevant effects. Compared to previous microglia gene knockout neuroimaging studies,[67–69] which have used smaller samples (7–20 mice per group) and detected large effects (Cohen's d = 0.85–2.2),[67–69] our sample size was substantially larger (34 mice per group with sexes combined) and provided 80% power to detect up to moderate effects (Cohen's d = 0.7). However, we acknowledge that smaller genotype effects below these thresholds may remain undetected, and thus the possibility of Type II error for subtle differences cannot be excluded.

Similarly to whole brain analyses, we did not observe any genotype-dependent changes to specific brain networks, including anxiety networks (**Figure 5**), which we hypothesised to be affected based on our previous behavioural results.[31] However, our

15

anxiety network connectivity null findings are internally consistent with the absence of an anxiety-like phenotype in the cohorts tested in this study. Our data combined with another recent null report for an anxiety-like effect in the EPM in *C3ar1*-deficient animals[34] suggests that *C3ar1* deficiency alone is not enough to result in anxiety-like behaviour or changes to anxiety networks.

Although we did not detect network-specific effects, *C3ar1*-deficient mice exhibited subtle but widespread increases in resting-state FC in voxel-wise seed-based analyses during adolescence across nearly all seeds examined, with a weaker effect persisting into adulthood (**Figure 6** and **Supplemental figures 9–11**). These increases in connectivity may be noise but they could reflect developmental alterations in circuit properties caused by the absence of C3aR1 that are not conclusively detectable by MRI. For now, we urge caution with this latter interpretation for two reasons that should be considered together. These connectivity changes were isolated findings—that is, they were not associated with any behavioural changes, nor were they accompanied by any structural alterations. This would be unexpected if a larger number of neurons were present due to, for example, a deficit in perinatal neuron phagocytosis as reported for *Cr3* knockouts.[69] Second, the voxel-wise seed-based analysis is the least robust presented here, as the observed changes were largely transient, weak, not confined to a specific subnetwork, and not corrected for multiple comparisons across seeds. Future studies investigating FC in *C3ar1*-deficient mice should incorporate repeated measures from the same individual during adolescence to improve robustness as well as assessing synaptic transmission more directly, for example by electrophysiology in brain slices, although it is still unclear which brain regions should be targeted currently with the latter approach.

Behavioural outcomes were unaffected by *C3ar1* deficiency

Neither anxiety-like behaviours nor locomotor activity showed significant differences between genotypes across multiple testing paradigms, apart from a small decrease in ambulation of *C3ar1*-deficient mice in the aversive central zone of the OF arena, which in the absence of a locomotor phenotype could index anxiety-like behaviour.[99] This latter change, however, was not reproducible across study cohorts and was no longer observed in the same study in the core of the OF arena. Tests for recognition memory and sensorimotor gating, NOR and PPI, also yielded null results.

Unlike previous studies of *C3ar1*-deficient mice, our study employed littermate control animals, meaning that wild-type mice were co-housed with their *C3ar1*-deficient siblings. This approach minimises potential environmental differences between groups, which is especially important in neurobehavioral studies where subtle environmental factors can significantly affect outcomes. While the use of littermate controls is widely regarded as best practice in such contexts,[38,100,101] it is not without its own potential confounds. For instance, abnormal behaviours exhibited by genetically altered animals can influence the behaviour of co-housed wild-type mice, particularly when the phenotype is pronounced, such as in cases of increased aggression.[83] However, as aggression has not been reported in *C3ar1*-deficient mice, and their previously described behavioural phenotype was not notably severe, we considered such an influence unlikely in our study, especially as the anxiety-like behaviour of our wild-type mice did not seem to depend on the number of *C3ar1*-deficient cage-mates (**Supplemental figure 12**).

16

The complement system plays an essential role in normal pregnancy and parturition.[102] A notable aspect of using a littermate design is that mixed-genotype litters are produced by breeding heterozygous parents, whereas in most previous studies of *C3ar1* deficiency, both the mother and offspring were homozygous knockouts. An exception is a report of hyperactivity in *C3ar1* knockout mice in which the knockouts were generated from heterozygous incrosses.[30] This raises the possibility that some behavioural effects in *C3ar1*-deficient mice (anxiety-like behaviour and a memory deficit) may have resulted from altered intrauterine environments or care by *C3ar1*-deficient mothers. If this is indeed the reason for the previously observed adult behavioural phenotypes, two scenarios should be considered. In the first, unlikely scenario, the *C3ar1*-deficient offspring are *uniquely sensitive* to C3aR1-dependent *in utero* conditions or maternal care deficits. In the second scenario, the adult phenotypes are not specific to *C3ar1*-deficiency meaning that wild-type mice would have been similarly affected. These scenarios can be tested by using pup transfer and *in-vitro* fertilisation experiments. For now, we were able to avoid measuring these non-specific effects on behaviour by using a littermate design.

The genetic background of mutants is another factor that varies between laboratories and is known to affect phenotypic expression. For example, heterozygous knockout of the autism-associated gene *CHD8* has varying effects in 33 sub-strains,[103] mirroring heterogeneity observed in human *CHD8*-haploinsufficiency. While that study identified significant variability across sub-strains, these profiles consistently differed from that of wild-type littermate controls. In contrast, our study found no robust genotype-dependent differences in the brain globally and across measures or in behaviour, apart from a single internally non-reproducible behavioural outcome measure, meaning that the effect of C3aR1 on behaviour would have to be entirely dependent on modifying genes or environmental factors.

Masking of a knockout phenotype can also occur through genetic compensation—an incompletely understood molecular process that leads to the upregulation of nearby and related genes, possibly through mutant RNA decay.[104] To rule this out, scRNA-Seq analysis would have to be conducted at every time-point and tissue of interest. For now, it is reassuring that in adult *C3ar1^tm1Cge/tm1Cge* hippocampus bulk RNA-Seq data, GPCRs do not appear to be upregulated at baseline.[105]

Finally, genetic drift could have precluded reproducibility of previously reported phenotypes. Mice accumulate spontaneous mutations that rapidly reach homozygosity within small colonies, speeding up drift, a phenomenon recognised as early as the 1980s.[35] So far, our current work is the first to study *C3ar1* deficiency in behaviour using a littermate design, which minimises the number of genetic loci that differ between the mutant and control mice, all of which could influence measured phenotypes.

Limitations

In this study, we provided high-level global data on *C3ar1*-deficient mice. While our study had notable strengths, including the use of a littermate design and the inclusion of female animals, it is not an exhaustive characterisation of the mutant.

17

While we measured brain region volumes, we cannot definitively address more reductionist questions, such as cellular composition which would have required single cell RNASeq or antibody staining and microscopy. Similarly, for axonal integrity analysis for which we used the proxy of dMRI-derived FA, the gold standard would have been electron microscopy. However, a more granular approach would have necessitated a trade-off with throughput—something that is hard to justify in the absence of strong hypotheses regarding the developmental expression pattern of *C3ar1*. Additionally, our fMRI analysis relied on a specific parcellation of the brain consisting of 36 regions, and different parcellations could yield varying results.[107,108] We encourage others exploring our datasets to therefore experiment with alternative parcellations.

It is important to note that rodent fMRI is typically performed under anaesthesia. We used a previously validated combined medetomidine and isoflurane anaesthesia selected for preserving maximum number of functional connections.[51] Nevertheless, anaesthesia can influence FC patterns. Medetomidine, in particular, has been reported to reduce inter-hemispheric FC,[109] and the combination with isoflurane may further alter connectivity signatures, particularly as it can stimulate the immune system[110] and therefore may hypothetically interact with the complement system. While there is no evidence that this protocol differentially affects wild-type and *C3ar1* knockout animals, it cannot be completely ruled out that *C3ar1* deficiency affects anaesthesia response in unforeseen ways, although this would be a more pressing concern in the presence of a strong *C3ar1*-dependent phenotype. It is also possible that our anaesthesia protocol may have masked a genotype effect. However, the absence of a consistent trend across measures supports the interpretation that this is a true null result.

Future directions

Aside from the role of C3aR1 in brain structure and function, many aspects of the basic biology of C3aR1 remain unclear, including its expression pattern in the healthy brain, with little information available on the cell types where it is expressed, its expression contexts and time-points. It is also unclear which G-proteins C3aR1 signals through in different brain cell types. Future studies could integrate toolkits like TRUPATH, a suite of $G\alpha\beta\gamma$ biosensors for analysing G-protein coupling preferences,[106] with transcriptomics to address these questions. This approach would be particularly valuable, as it could enable the use of chemogenetics to activate the same G-protein as C3aR1 in specific cell types and contexts to study its function. Only after these fundamental investigations have been completed should *C3ar1* deficiency be examined at the behavioural level—particularly following immune challenges known to activate complement in the brain during critical periods of development.

Data and Code availability:

Data availability: All behavioural videos have been deposited via Zenodo. Due to repository size limitations, datasets were divided by both experimental cohort and behavioural task;
https://doi.org/10.5281/zenodo.17100928 (Cohort 1 open field),
https://doi.org/10.5281/zenodo.17107902 (Cohort 1 elevated plus maze),
https://doi.org/10.5281/zenodo.17113481 (Cohort 2 open field and elevated plus maze) and

18

https://doi.org/10.5281/zenodo.17113949 (Cohort 2 novel object recognition training and test videos).

Raw MRI images and relevant metadata can be found on OpenNeuro:
https://openneuro.org/datasets/ds006663/versions/1.0.1 (Cohort 1, doi:10.18112/openneuro.ds006663.v1.0.1)
https://openneuro.org/datasets/ds006670/versions/1.0.0 (Cohort 2, doi:10.18112/openneuro.ds006670.v1.0.0)
Intermediary analysis files, including preprocessed data, are maintained alongside the code at https://github.com/hannalemmik/C3ar1_longitudinal_MRI_paper_2025.

Code availability: The analysis code used to reproduce all figures in this manuscript is available at https://github.com/hannalemmik/C3ar1_longitudinal_MRI_paper_2025. Additional MRI processing scripts are available upon request from Eugene Kim.

Competing interests statement: The authors declare no competing interests.

References

1. Chaplin H Jr. Review: the burgeoning history of the complement system 1888-2005. *Immunohematology*. 2020;21(3):85-93.

2. Kunz N, Kemper C. Complement has brains-do intracellular complement and immunometabolism cooperate in tissue homeostasis and behavior? *Front Immunol*. 2021;12:629986.

3. West EE, Kemper C. Complosome - the intracellular complement system. *Nat Rev Nephrol*. 2023;19(7):426-439.

4. Stevens B, Allen NJ, Vazquez LE, et al. The Classical Complement Cascade Mediates CNS Synapse Elimination. *Cell*. 2007;131(6):1164-1178.

5. Hong S, Beja-Glasser VF, Nfonoyim BM, et al. Complement and microglia mediate early synapse loss in Alzheimer mouse models. *Science*. 2016;352(6286):712-716.

6. Sekar A, Bialas AR, de Rivera H, et al. Schizophrenia risk from complex variation of complement component 4. *Nature*. 2016;530(7589):177-183.

7. McCutcheon RA, Reis Marques T, Howes OD. Schizophrenia-an overview. *JAMA Psychiatry*. 2020;77(2):201-210.

19

8. Howes OD, Bukala BR, Beck K. Schizophrenia: from neurochemistry to circuits, symptoms and treatments. *Nat Rev Neurol*. 2024;20(1):22-35.

9. Vita A, De Peri L, Deste G, Sacchetti E. Progressive loss of cortical gray matter in schizophrenia: a meta-analysis and meta-regression of longitudinal MRI studies. *Transl Psychiatry*. 2012;2(11):e190.

10. Osimo EF, Beck K, Reis Marques T, Howes OD. Synaptic loss in schizophrenia: a meta-analysis and systematic review of synaptic protein and mRNA measures. *Mol Psychiatry*. 2019;24(4):549-561.

11. Schizophrenia Working Group of the Psychiatric Genomics Consortium. Biological insights from 108 schizophrenia-associated genetic loci. *Nature*. 2014;511(7510):421-427.

12. Baum ML, Wilton DK, Fox RG, et al. CSMD1 regulates brain complement activity and circuit development. *Brain Behav Immun*. Published online March 27, 2024. doi:10.1016/j.bbi.2024.03.041

13. Yilmaz M, Yalcin E, Presumey J, et al. Overexpression of schizophrenia susceptibility factor human complement C4A promotes excessive synaptic loss and behavioral changes in mice. *Nat Neurosci*. 2021;24(2):214-224.

14. O'Connell KS, Sønderby IE, Frei O, et al. Association between complement component 4A expression, cognitive performance and brain imaging measures in UK Biobank. *Psychol Med*. 2021;52(15):1-11.

15. Byrne JF, Healy C, Föcking M, et al. Plasma complement and coagulation proteins as prognostic factors of negative symptoms: An analysis of the NAPLS 2 and 3 studies. *Brain Behav Immun*. 2024;119:188-196.

16. Rodriguez P, Laskowski LJ, Pallais JP, et al. Functional profiling of the G protein-coupled receptor C3aR1 reveals ligand-mediated biased agonism. *J Biol Chem*. 2023;300(1):105549.

17. Hauser AS, Attwood MM, Rask-Andersen M, Schiöth HB, Gloriam DE. Trends in GPCR drug discovery: new agents, targets and indications. *Nat Rev Drug Discov*. 2017;16(12):829-842.

18. Hammond TR, Dufort C, Dissing-Olesen L, et al. Single-Cell RNA Sequencing of Microglia throughout the Mouse Lifespan and in the Injured Brain Reveals Complex Cell-State Changes. *Immunity*. 2019;50(1):253-271.e6.

19. Tasic B, Menon V, Nguyen TN, et al. Adult mouse cortical cell taxonomy revealed by single cell transcriptomics. *Nat Neurosci*. 2016;19(2):335-346.

20. Coulthard LG, Hawksworth OA, Conroy J, Lee JD, Woodruff TM. Complement C3a receptor modulates embryonic neural progenitor cell proliferation and cognitive performance. *Mol Immunol*. 2018;101:176-181.

20

21. Bénard M, Raoult E, Vaudry D, et al. Role of complement anaphylatoxin receptors (C3aR, C5aR) in the development of the rat cerebellum. *Mol Immunol*. 2008;45(14):3767-3774.

22. Gnanaguru G, Tabor SJ, Bonilla GM, et al. Microglia refine developing retinal astrocytic and vascular networks through the complement C3/C3aR axis. *Development*. 2023;150(5). doi:10.1242/dev.201047

23. Gedam M, Comerota MM, Propson NE, et al. Complement C3aR depletion reverses HIF-1α-induced metabolic impairment and enhances microglial response to Aβ pathology. *J Clin Invest*. 2023;133(12). doi:10.1172/JCI167501

24. Ge TQ, Guan PP, Wang P. Complement 3a induces the synapse loss via C3aR in mitochondria-dependent NLRP3 activating mechanisms during the development and progression of Alzheimer's disease. *Neurosci Biobehav Rev*. 2024;165(105868):105868.

25. Zheng J, Lu J, Mei S, et al. Ceria nanoparticles ameliorate white matter injury after intracerebral hemorrhage: microglia-astrocyte involvement in remyelination. *J Neuroinflammation*. 2021;18(1):43.

26. Lian H, Yang L, Cole A, et al. NFκB-activated astroglial release of complement C3 compromises neuronal morphology and function associated with Alzheimer's disease. *Neuron*. 2015;85(1):101-115.

27. Vasek MJ, Garber C, Dorsey D, et al. A complement-microglial axis drives synapse loss during virus-induced memory impairment. *Nature*. 2016;534(7608):538-543.

28. Chew G, Petretto E. Transcriptional Networks of Microglia in Alzheimer's Disease and Insights into Pathogenesis. *Genes* . 2019;10(10). doi:10.3390/genes10100798

29. Westacott LJ, Haan N, Evison C, et al. Dissociable effects of complement C3 and C3aR on survival and morphology of adult born hippocampal neurons, pattern separation, and cognitive flexibility in male mice. *Brain Behav Immun*. 2021;98:136-150.

30. Pozo-Rodrigálvarez A, Ollaranta R, Skoog J, Pekny M, Pekna M. Hyperactive Behavior and Altered Brain Morphology in Adult Complement C3a Receptor Deficient Mice. *Front Immunol*. 2021;12:406.

31. Westacott LJ, Humby T, Haan N, et al. Complement C3 and C3aR mediate different aspects of emotional behaviours; relevance to risk for psychiatric disorder. *Brain Behav Immun*. 2022;99:70-82.

32. Crider A, Feng T, Pandya CD, et al. Complement component 3a receptor deficiency attenuates chronic stress-induced monocyte infiltration and depressive-like behavior. *Brain Behav Immun*. 2018;70:246-256.

33. Zhang MM, Guo MX, Zhang QP, et al. IL-1R/C3aR signaling regulates synaptic pruning in the prefrontal cortex of depression. *Cell Biosci*. 2022;12(1):90.

21

34. Sun R, Tang MY, Yang D, et al. C3aR in the medial prefrontal cortex modulates the susceptibility to LPS-induced depressive-like behaviors through glutamatergic neuronal excitability. *Prog Neurobiol*. Published online April 17, 2024:102614.

35. Fitch WM, Atchley WR. Evolution in inbred strains of mice appears rapid. *Science*. 1985;228(4704):1169-1175.

36. Crews D, Rushworth D, Gonzalez-Lima F, Ogawa S. Litter environment affects behavior and brain metabolic activity of adult knockout mice. *Front Behav Neurosci*. 2009;3:12.

37. Jiménez JA, Zylka MJ. Controlling litter effects to enhance rigor and reproducibility with rodent models of neurodevelopmental disorders. *J Neurodev Disord*. 2021;13(1):2.

38. Valiquette V, Guma E, Cupo L, et al. Examining litter specific variability in mice and its impact on neurodevelopmental studies. *Neuroimage*. 2023;269:119888.

39. Westacott LJ, Wilkinson LS. Complement Dependent Synaptic Reorganisation During Critical Periods of Brain Development and Risk for Psychiatric Disorder. *Front Neurosci*. 2022;16:840266.

40. Paus T, Keshavan M, Giedd JN. Why do many psychiatric disorders emerge during adolescence? *Nat Rev Neurosci*. 2008;9(12):947-957.

41. Chan SY, Fitzgerald E, Ngoh ZM, et al. Examining the associations between microglia genetic capacity, early life exposures and white matter development at the level of the individual. *Brain Behav Immun*. 2024;119:781-791.

42. Falangola MF, Dhiman S, Voltin J, Jensen JH. Quantitative microglia morphological features correlate with diffusion MRI in 2-month-old 3xTg-AD mice. *Magn Reson Imaging*. 2023;103:8-17.

43. Zhu H, Qiu C, Meng Y, et al. Altered topological properties of brain networks in social anxiety disorder: A resting-state functional MRI study. *Sci Rep*. 2017;7(1):43089.

44. Forlim CG, Klock L, Gallinat J, Kühn S. Altered resting-state functional connectivity in a thalamo-cortico-cerebellar network in patients with schizophrenia. *Sci Rep*. 2024;14(1):26284.

45. Hadley JA, Kraguljac NV, White DM, Ver Hoef L, Tabora J, Lahti AC. Change in brain network topology as a function of treatment response in schizophrenia: a longitudinal resting-state fMRI study using graph theory. *NPJ Schizophr*. 2016;2(1):16014.

46. Humbles AA, Lu B, Nilsson CA, et al. A role for the C3a anaphylatoxin receptor in the effector phase of asthma. *Nature*. 2000;406(6799):998-1001.

22

47. Semaan SJ, Kauffman AS. Daily successive changes in reproductive gene expression and neuronal activation in the brains of pubertal female mice. *Mol Cell Endocrinol*. 2015;401:84-97.

48. Brust V, Schindler PM, Lewejohann L. Lifetime development of behavioural phenotype in the house mouse (Mus musculus). *Front Zool*. 2015;12 Suppl 1(S1):S17.

49. Pintér O, Beda Z, Csaba Z, Gerendai I. Differences in the onset of puberty in selected inbred mouse strains. *Endocrine Abstracts*. 2007;14. Accessed April 14, 2025. https://www.endocrine-abstracts.org/ea/0014/ea0014p617

50. Serrano ME, Kim E, Siow B, et al. Investigating brain alterations in the Dp1Tyb mouse model of Down syndrome - ScienceDirect. *Neurobiol Dis*. 2023;188:106336.

51. Grandjean J, Schroeter A, Batata I, Rudin M. Optimization of anesthesia protocol for resting-state fMRI in mice based on differential effects of anesthetics on functional connectivity patterns. *Neuroimage*. 2014;102 Pt 2:838-847.

52. Wood TC, Simmons C, Hurley SA, et al. Whole-brain ex-vivo quantitative MRI of the cuprizone mouse model. *PeerJ*. 2016;4:e2632.

53. Kim E, Carreira Figueiredo I, Simmons C, et al. Mapping acute neuroinflammation in vivo with diffusion-MRI in rats given a systemic lipopolysaccharide challenge. *Brain Behav Immun*. 2023;113:289-301.

54. Lerch JP, Gazdzinski L, Germann J, Sled JG, Henkelman RM, Nieman BJ. Wanted dead or alive? The tradeoff between in-vivo versus ex-vivo MR brain imaging in the mouse. *Front Neuroinform*. 2012;0(MARCH):6.

55. Wang Q, Ding SL, Li Y, et al. The Allen Mouse Brain Common Coordinate Framework: A 3D Reference Atlas. *Cell*. 2020;181(4):936-953.e20.

56. Rubinov M, Sporns O. Complex network measures of brain connectivity: uses and interpretations. *Neuroimage*. 2010;52(3):1059-1069.

57. Grandjean J, Canella C, Anckaerts C, et al. Common functional networks in the mouse brain revealed by multi-centre resting-state fMRI analysis. *Neuroimage*. 2020;205. doi:10.1016/J.NEUROIMAGE.2019.116278

58. Sforazzini F, Schwarz AJ, Galbusera A, Bifone A, Gozzi A. Distributed BOLD and CBV-weighted resting-state networks in the mouse brain. *Neuroimage*. 2014;87:403-415.

59. Tao J, Zhao J, Qi XM, Wu YG. Complement-mediated M2/M1 macrophage polarization may be involved in crescent formation in lupus nephritis. *Int Immunopharmacol*. 2021;101(Pt A):108278.

60. Mommert S, Aslan D, Ratz L, Stark H, Gutzmer R, Werfel T. The anaphylatoxin C3a receptor expression on human M2 macrophages is down-regulated by

23

stimulating the histamine H4 receptor and the IL-4 receptor. *J Innate Immun*. 2018;10(4):349-362.

61. Mamane Y, Chung Chan C, Lavallee G, et al. The C3a anaphylatoxin receptor is a key mediator of insulin resistance and functions by modulating adipose tissue macrophage infiltration and activation. *Diabetes*. 2009;58(9):2006-2017.

62. Guma E, Beauchamp A, Liu S, et al. Comparative neuroimaging of sex differences in human and mouse brain anatomy. *Elife*. 2024;13. doi:10.7554/eLife.92200

63. Gorski RA, Gordon JH, Shryne JE, Southam AM. Evidence for a morphological sex difference within the medial preoptic area of the rat brain. *Brain Res*. 1978;148(2):333-346.

64. Hines M, Allen LS, Gorski RA. Sex differences in subregions of the medial nucleus of the amygdala and the bed nucleus of the stria terminalis of the rat. *Brain Res*. 1992;579(2):321-326.

65. Friedrich P, Fraenz C, Schlüter C, et al. The relationship between axon density, myelination, and fractional anisotropy in the human corpus callosum. *Cereb Cortex*. 2020;30(4):2042-2056.

66. Gretenkord S, Kostka JK, Hartung H, et al. Coordinated electrical activity in the olfactory bulb gates the oscillatory entrainment of entorhinal networks in neonatal mice. *PLoS Biol*. 2019;17(1):e2006994.

67. Filipello F, Morini R, Corradini I, et al. The microglial innate immune receptor TREM2 is required for synapse elimination and normal brain connectivity. *Immunity*. 2018;48(5):979-991.e8.

68. Zhan Y, Paolicelli RC, Sforazzini F, et al. Deficient neuron-microglia signaling results in impaired functional brain connectivity and social behavior. *Nat Neurosci*. 2014;17(3):400-406.

69. Deivasigamani S, Miteva MT, Natale S, et al. Microglia complement signaling promotes neuronal elimination and normal brain functional connectivity. *Cereb Cortex*. 2023;33(21):10750-10760.

70. Bassett DS, Bullmore ET, Meyer-Lindenberg A, Apud JA, Weinberger DR, Coppola R. Cognitive fitness of cost-efficient brain functional networks. *Proc Natl Acad Sci U S A*. 2009;106(28):11747-11752.

71. Bullmore E, Sporns O. Complex brain networks: graph theoretical analysis of structural and functional systems. *Nat Rev Neurosci*. 2009;10(3):186-198.

72. Berlot R, Metzler-Baddeley C, Ikram MA, Jones DK, O'Sullivan MJ. Global efficiency of structural networks mediates cognitive control in Mild Cognitive Impairment. *Front Aging Neurosci*. 2016;8:292.

24

73. Hawkins R, Shatil AS, Lee L, et al. Reduced global efficiency and random network features in patients with relapsing-remitting multiple sclerosis with cognitive impairment. *AJNR Am J Neuroradiol*. 2020;41(3):449-455.

74. Jiang W, Zhou Z, Li G, et al. Mapping the evolution of regional brain network efficiency and its association with cognitive abilities during the first twenty-eight months of life. *Dev Cogn Neurosci*. 2023;63(101284):101284.

75. Zalesky A, Fornito A, Bullmore ET. Network-based statistic: identifying differences in brain networks. *Neuroimage*. 2010;53(4):1197-1207.

76. Coutinho JF, Fernandesl SV, Soares JM, Maia L, Gonçalves ÓF, Sampaio A. Default mode network dissociation in depressive and anxiety states. *Brain Imaging Behav*. 2016;10(1):147-157.

77. Geng H, Li X, Chen J, Li X, Gu R. Decreased intra- and inter-salience network functional connectivity is related to trait anxiety in adolescents. *Front Behav Neurosci*. 2015;9:350.

78. Schimmelpfennig J, Topczewski J, Zajkowski W, Jankowiak-Siuda K. The role of the salience network in cognitive and affective deficits. *Front Hum Neurosci*. 2023;17:1133367.

79. Hikishima K, Tsurugizawa T, Kasahara K, Takagi R, Yoshinaka K, Nitta N. Brain-wide mapping of resting-state networks in mice using high-frame rate functional ultrasound. *Neuroimage*. 2023;279(120297):120297.

80. Crawley JN. What's wrong with my mouse?: behavioral phenotyping of transgenic and knockout mice. Published online 2007. https://books.google.com/books?hl=en&lr=&id=rjP6DwAAQBAJ&oi=fnd&pg=PR9&ots=_nB47H3YQO&sig=ZWrrfhxl6qbJNOD95BZFAWrQ7uM

81. Ludewig K, Geyer MA, Vollenweider FX. Deficits in prepulse inhibition and habituation in never-medicated, first-episode schizophrenia. *Biol Psychiatry*. 2003;54(2):121-128.

82. Mena A, Ruiz-Salas JC, Puentes A, Dorado I, Ruiz-Veguilla M, De la Casa LG. Reduced Prepulse Inhibition as a Biomarker of Schizophrenia. *Front Behav Neurosci*. 2016;10:202.

83. Kalbassi S, Bachmann SO, Cross E, Roberton VH, Baudouin SJ. Male and Female Mice Lacking Neuroligin-3 Modify the Behavior of Their Wild-Type Littermates. *eNeuro*. 2017;4(4). doi:10.1523/ENEURO.0145-17.2017

84. Qiu LR, Fernandes DJ, Szulc-Lerch KU, et al. Mouse MRI shows brain areas relatively larger in males emerge before those larger in females. *Nat Commun*. 2018;9(1):1-15.

85. de Courten-Myers GM. The human cerebral cortex: gender differences in structure and function. *J Neuropathol Exp Neurol*. 1999;58(3):217-226.

25

86. Wang Y, Pandey S, Weber M, et al. Complement C3aR deletion does not attenuate neurodegeneration in a tauopathy model or alter acute inflammation-induced gene expression changes in the brain. *bioRxiv*. Published online June 17, 2025:2025.06.16.660026. doi:10.1101/2025.06.16.660026

87. Quell KM, Karsten CM, Kordowski A, et al. Monitoring C3aR Expression Using a Floxed tdTomato-C3aR Reporter Knock-in Mouse. *The Journal of Immunology*. 2017;199(2):688-706.

88. Tasic B, Yao Z, Graybuck LT, et al. Shared and distinct transcriptomic cell types across neocortical areas. *Nature*. 2018;563(7729):72-78.

89. Brouwer RM, Mandl RCW, Schnack HG, et al. White matter development in early puberty: a longitudinal volumetric and diffusion tensor imaging twin study. *PLoS One*. 2012;7(4):e32316.

90. Hagmann P, Sporns O, Madan N, et al. White matter maturation reshapes structural connectivity in the late developing human brain. *Proc Natl Acad Sci U S A*. 2010;107(44):19067-19072.

91. Reynolds JE, Grohs MN, Dewey D, Lebel C. Global and regional white matter development in early childhood. *Neuroimage*. 2019;196:49-58.

92. Piekarski DJ, Zahr NM, Zhao Q, et al. White matter microstructural integrity continues to develop from adolescence to young adulthood in mice and humans: Same phenotype, different mechanism. *Neuroimage Rep*. 2023;3(3). doi:10.1016/j.ynirp.2023.100179

93. Chahboune H, Ment LR, Stewart WB, Ma X, Rothman DL, Hyder F. Neurodevelopment of C57B/L6 mouse brain assessed by in vivo diffusion tensor imaging. *NMR Biomed*. 2007;20(3):375-382.

94. Rojo R, Raper A, Ozdemir DD, et al. Deletion of a Csf1r enhancer selectively impacts CSF1R expression and development of tissue macrophage populations. *Nat Commun*. 2019;10(1):3215.

95. Kiani Shabestari S, Morabito S, Danhash EP, et al. Absence of microglia promotes diverse pathologies and early lethality in Alzheimer's disease mice. *Cell Rep*. 2022;39(11):110961.

96. Caseras X, Simmonds E, Pardiñas AF, et al. Common risk alleles for schizophrenia within the major histocompatibility complex predict white matter microstructure. *Transl Psychiatry*. 2024;14(1):194.

97. Koenis MMG, Brouwer RM, Swagerman SC, van Soelen ILC, Boomsma DI, Hulshoff Pol HE. Association between structural brain network efficiency and intelligence increases during adolescence. *Hum Brain Mapp*. 2018;39(2):822-836.

98. Cai L, Dong Q, Niu H. The development of functional network organization in early childhood and early adolescence: A resting-state fNIRS study. *Dev Cogn Neurosci*. 2018;30:223-235.

26

99. Prut L, Belzung C. The open field as a paradigm to measure the effects of drugs on anxiety-like behaviors: a review. *Eur J Pharmacol*. 2003;463(1-3):3-33.

100. Holmdahl R, Malissen B. The need for littermate controls. *Eur J Immunol*. 2012;42(1):45-47.

101. Bailey KR, Rustay NR, Crawley JN. Behavioral phenotyping of transgenic and knockout mice: practical concerns and potential pitfalls. *ILAR J*. 2006;47(2):124-131.

102. Girardi G, Lingo JJ, Fleming SD, Regal JF. Essential role of complement in pregnancy: From implantation to parturition and beyond. *Front Immunol*. 2020;11:1681.

103. Tabbaa M, Knoll A, Levitt P. Mouse population genetics phenocopies heterogeneity of human Chd8 haploinsufficiency. *Neuron*. 2023;111(4):539-556.e5.

104. El-Brolosy MA, Kontarakis Z, Rossi A, et al. Genetic compensation triggered by mutant mRNA degradation. *Nature*. 2019;568(7751):193-197.

105. Litvinchuk A, Wan YW, Swartzlander DB, et al. Complement C3aR inactivation attenuates tau pathology and reverses an immune network deregulated in tauopathy models and Alzheimer's disease. *Neuron*. 2018;100(6):1337.

106. Olsen RHJ, DiBerto JF, English JG, et al. TRUPATH, an open-source biosensor platform for interrogating the GPCR transducerome. *Nat Chem Biol*. 2020;16(8):841-849.

107. Thirion B, Varoquaux G, Dohmatob E, Poline JB. Which fMRI clustering gives good brain parcellations? *Front Neurosci*. 2014;8:167.

108. Zalesky A, Fornito A, Harding IH, et al. Whole-brain anatomical networks: does the choice of nodes matter? *Neuroimage*. 2010;50(3):970-983.

109. Bukhari Q, Schroeter A, Cole DM, Rudin M. Resting state fMRI in mice reveals anesthesia specific signatures of brain functional networks and their interactions. *Front Neural Circuits*. 2017;11:5.

110. Wu X, Lu Y, Dong Y, et al. The inhalation anesthetic isoflurane increases levels of proinflammatory TNF-α, IL-6, and IL-1β. *Neurobiol Aging*. 2012;33(7):1364-1378.

Figure 1 | *C3ar1^tm1Cge/tm1Cge* **mice lack detectable** *C3ar1* **mRNA.** (**A**) Schematic shows *C3ar1* mRNA with its only protein coding exon and the design of the 79 bp PCR amplicon which targets an exon-1/5' untranslated region (UTR) and exon-2 junction of the canonical *C3ar1* wildtype transcript. Also shown is another 372 bp amplicon which targets a region downstream of the deletion and after an alternative start codon. The start of exon 2 is deleted in *C3ar1^tm1Cge/tm1Cge* mice, so PCR should result in no amplification. Similarly, if no alternative transcript is present, there should be no

27

amplification. (**B–C**) Gel images show PCR products of cDNA from bone-marrow derived interleukin 4 (IL4)-induced M2-like macrophages. Each sample well has a 297 bp Glyceraldehyde 3-phosphate dehydrogenase (*Gapdh*) control band. -/- = *C3ar1*$^{tm1Cge/tm1Cge}$, +/+ = *C3ar1*$^{+/+}$. NEG: no reverse transcriptase negative control carried over from cDNA synthesis. (**B**) Canonical transcript. (**C**) Hypothesised alternative transcript. The bands appear hollow due to over-saturation. Original uncropped gel images can be found in **Supplemental figure 3**. (**D, E**) qPCR of cDNA from bone marrow-derived macrophages: (**D**) M0 and (**E**) M2 from *C3ar1*$^{tm1Cge/tm1Cge}$ mice and wildtype littermates ($N = 4$ mice for each genotype), Kruskal Wallis test M0 $p < 0.05$, M2 $p < 0.05$. Point plots show mean ± 95% CI, data points for individual mice are shown. *Hprt* = Hypoxanthine-Guanine Phosphoribosyltransferase 1 (housekeeping gene).

Figure 2 | Sex but not *C3ar1* status influences regional brain volume. (**A**) Schematic of the MRI study shown in (**D–G**). 69 mice were scanned twice *in vivo*, in adolescence at ~postnatal day (PND) 30 (range 27-31) and at adulthood ~PND90 (range 81-92), as well as once *ex vivo* after sacrifice after the adulthood scanning session. Behavioural tests were carried out before the adulthood scanning session. EPM = elevated plus maze, OF = open field. (**B**) Total brain volume in adolescence. Two-way ANOVA, genotype, sex, genotype * sex, $F_{[1,65]} = 0.35, 16.72, 3.26, p = 0.56, <0.001, 0.76$. (**C**) Total brain volume in adulthood. Two-way ANOVA, genotype, sex, genotype * sex, $F_{[1,65]} = 0.74, 0.26, 3.33, p = 0.39, 0.61, 0.07$. (**B–C**) Data presented as mean ± 95% CI. Each datapoint represents an individual mouse. (**D**) Panels showing relative regional volume changes (%) overlaid on study-specific coronal templates (grey). Red hues signify areas larger in *C3ar1*$^{tm1Cge/tm1Cge}$ (**i–ii**) or females (**iii–iv**) and blue hues signify areas larger in *C3ar1*$^{+/+}$ (**i–ii**) or males (**iii–iv**). Transparency of the colour overlay shows the statistical significance, ranging from family-wise error rate (FWER)-corrected voxel-wise *t* test *p* value 0.5 to 0 (transparent to opaque, respectively). Areas where FWE-corrected *p* value < 0.05 are demarcated with a black line, and where the *p* value > 0.5 are grey (no overlay), meaning that in adolescence genotype comparison (**i**), no voxels had a *p* value < 0.5. The locations of the coronal slices in relation to bregma in the left most column from top: -7.6, -4.6, -1.6, 1.4 mm. *C3ar1*$^{+/+}$ $N = 35$, 17 males and 18 females; *C3ar1*$^{tm1Cge/tm1Cge}$ $N = 34$, 18 males and 16 females. ACAd = dorsal anterior cingulate cortex, AI = agranular insular cortex, BST = bed nucleus of stria terminalis, CA = cornu ammonis, CP = caudoputamen, DG = dentate gyrus, MEA = medial amygdala, MEPO = medial preoptic nucleus, MOs = secondary motor cortex (MOs), MPO = medial preoptic area, MS = medial septum, OB = olfactory bulb, PAG = periaqueductal grey, PRT = pretectal area, SC = superior colliculus, SSp = primary somatosensory cortex. (**E**) Regional volume coefficient of variation (CV) in adolescence *in vivo*. (**F**) CV in adulthood *in vivo*. (**G**) CV in adulthood *ex vivo*. (**E–G**) Each data point represents the CV calculated for an individual brain region, using data from all animals; thus, $N = 66$ regions (all atlas regions excluding cerebrospinal fluid areas). Data are shown with quartiles, whiskers show the extent of the distribution. Kruskal Wallis *p* values, all ns. D. hipp = dorsal hippocampus, v. hipp = ventral hippocampus.

Figure 3 | Fractional anisotropy does not depend on *C3ar1* status but increases with age. (**A**) Panels showing voxel-wise fractional anisotropy analysis (voxel-wise *t* tests) in adolescence (top) and adulthood (bottom) corrected for FWER. There are no significant voxels (no black contour) where genotype effect is significant ($p < 0.05$). CC

= corpus callosum, OPT = optic tract. (**B**) *In vivo* ROI-based median fractional anisotropy (FA) values in white matter regions for (**i**) adolescence, (**ii**) adulthood and (**iii**) change over time (adulthood − adolescence). Two-sided one-sample *t* test (difference from 0) *p* values that were adjusted with Benjamini-Hochberg (BH) procedure (### *p* value < 0.001). (**Bi–iii**) Mixed ANOVA with genotype and genotype-by-region interaction effects, all ns. Data are presented as mean ± 95% CI. (**A–B**) Adolescence: *C3ar1*$^{+/+}$ $N = 34$, 16 males and 18 females; *C3ar1*$^{tm1Cge/tm1Cge}$ $N = 33$, 17 males and 16 females. Adulthood: *C3ar1*$^{+/+}$ $N = 31$ (15 males and 16 females); *C3ar1*$^{tm1Cge/tm1Cge}$ $N = 26$ (13 males and 13 females). Change: *C3ar1*$^{+/+}$ $N = 30$ (14 males and 16 females); *C3ar1*$^{tm1Cge/tm1Cge}$ $N = 25$ (12 males and 13 females).

Figure 4 | Global functional connectivity is not changed in *C3ar1*-deficient mice. Functional connectivity, clustering coefficient and global efficiency at decreasing graph sparsity levels in adolescence (**A–C**), and adulthood (**D–F**), and change over time (**G–I**). (**A–I**) Statistical significance was determined with sexes combined using AUC permutation testing (10000 iterations) and the resulting *p* values were corrected for multiplicity with the Bonferroni method ($N = 3$ tests per outcome measure). Adolescence: *C3ar1*$^{+/+}$ $N = 32$ (15 males, 17 females); *C3ar1*$^{tm1Cge/tm1Cge}$ $N = 32$ (18 males, 14 females); Adulthood: *C3ar1*$^{+/+}$ $N = 33$ (16 males, 17 females) and *C3ar1*$^{tm1Cge/tm1Cge}$ $N = 32$ (17 males, 15 females); change: *C3ar1*$^{+/+}$ $N = 30$ (14 males and 16 females); *C3ar1*$^{tm1Cge/tm1Cge}$ $N = 31$ (17 males and 14 females). Data are shown as mean ± 95% CI. (**G–I**) Two-sided one-sample *t* tests (difference from 0) for global connectivity changes at each sparsity level with genotypes combined, corrected using the BH procedure ($N = 10$ sparsity levels), # = adjusted *p* value < 0.05. Coef = coefficient.

Figure 5 | *C3ar1*-deficiency does not influence functional brain networks. (**A**) Thresholded adjacency matrices comparing *C3ar1*$^{+/+}$ and *C3ar1*$^{tm1Cge/tm1Cge}$ micewhere $|t| \geq 2$ in adolescence and adulthood, and the change between time points. No connections with $|t| \geq 2$ remained significant after the false discovery rate (FDR) correction. Additionally, the number of connections in the $|t| \geq 2$ adjacency matrix components were not significant when assessed using network-based statistics (NBS) correction. (**B**) Nodal strength (mean absolute connectivity) of *a priori* anxiety-related seeds (e.g. L cingulate cortex correlation coefficients with all other regions). *P* values were calculated using a mixed ANOVA with between-subjects factor of genotype and within-subjects factor of region. Only the region effect was significant at both time-points (both *p* values < 0.001, $\eta_p^2 = 0.69$ in adolescence and $\eta_p^2 = 0.73$ in adulthood). (**C**) Functional connectivity (FC) and global efficiency (GE) were analysed using mixed effects linear models with genotype, time point (adolescence and adulthood) and their interaction as fixed effects and mouse ID as a random effect. Analyses were run separately for each network, corrected with the Bonferroni method (three tests). All *p* values = ns. (**A–C**) Adolescence: *C3ar1*$^{+/+}$ $N = 32$ (15 males, 17 females); *C3ar1*$^{tm1Cge/tm1Cge}$ $N = 32$ (18 males, 14 females); Adulthood: *C3ar1*$^{+/+}$ $N = 33$ (16 males, 17 females) and *C3ar1*$^{tm1Cge/tm1Cge}$ $N = 32$ (17 males, 15 females).

Figure 6 | Examples of seed-based FC maps. Shown are voxel-wise group differences between *C3ar1*$^{tm1Cge/tm1Cge}$ and *C3ar1*$^{+/+}$ mice (using *t* tests) with seeds placed in the left ventral hippocampus and left prefrontal cortex in adolescence and adulthood datasets. The dual scale bar displays contrast value on the x-axis and TFCE *p*-values

29

(transformed $0.81 - p$) on the y-axis. The transformed *p*-values have been re-scaled to range from 0 to 1 for visualisation, with darker colours representing greater statistical significance. Black outlines demarcate regions where TFCE *p*-values are below 0.05. Adolescence: *C3ar1*$^{+/+}$ $N = 32$ (15 males, 17 females); *C3ar1*$^{tm1Cge/tm1Cge}$ N = 32 (18 males, 14 females); Adulthood: *C3ar1*$^{+/+}$ $N = 33$ (16 males, 17 females) and *C3ar1*$^{tm1Cge/tm1Cge}$ $N = 32$ (17 males, 15 females).

Figure 7 | *C3ar1* deficiency does not cause behavioural abnormalities. (**A**) Cohort 1 OF distance travelled in one-minute bins plotted as median ± interquartile range, fitted with exponential decay curves; dotted lines show the asymptote and the time animals reach 95% stability in distance travelled per minute. Effects of time bin, genotype and their interaction tested with two-way ANOVA; only time was significant ($p < 0.01$). (**B–F**) Cohort 1 OF and EPM: anxiety-like outcomes for *C3ar1*$^{+/+}$ and *C3ar1*$^{tm1Cge/tm1Cge}$ mice, separated by sex. Statistical comparisons made using two-way ANOVA (genotype × sex) for each metric; all effects ns so no post-hoc comparisons were performed. Individual *p* values can be found in **Supplemental table 5.** (**G**) Prepulse inhibition (PPI) in Cohort 2. Individuals plotted per genotype, and sexes are separated only for visualisation. PPI increased with increasing prepulse intensity in both genotypes (paired *t* tests p value ### < 0.001); no genotype differences by Student's *t* tests (*C3ar1*$^{+/+}$ vs *C3ar1*$^{tm1Cge/tm1Cge}$ all *p* values > 0.05). Dashed line marks inhibition threshold.(**H–I**) Z-scored locomotion and anxiety metrics for *C3ar1*$^{tm1Cge/tm1Cge}$ mice normalised to *C3ar1*$^{+/+}$ mean, showing Cohorts 1 and 2. (**J**) Novel object recognition recall 1 h after acquisition in Cohort 2. Sexes are separated only for visualisation. Both genotypes showed novelty preference (one-sample *t* test, value > 50/chance, # = $p < 0.05$, ## = $p < 0.01$ ### = $p < 0.001$). There were no differences between groups (*C3ar1*$^{+/+}$ vs *C3ar1*$^{tm1Cge/tm1Cge}$ Student's *t* test $t_{[37]} = 0.42$, $p = 0.67$). (**A–I**). Experimental units are individual mice. Cohort 1: *C3ar1*$^{tm1Cge/tm1Cge}$ $N = 34$ (18 male, 16 female), *C3ar1*$^{+/+}$ $N = 35$ (17 male, 18 female), except for EPM where one *C3ar1*$^{tm1Cge/tm1Cge}$ mouse (male) and two *C3ar1*$^{+/+}$ mice (one male, one female) were removed from analysis due to falling off the open arm. Cohort 2: *C3ar1*$^{tm1Cge/tm1Cge}$ $N = 20$, *C3ar1*$^{+/+}$ $N = 19$ (males and females combined), except for EPM where two female *C3ar1*$^{tm1Cge/tm1Cge}$ mice and one male *C3ar1*$^{+/+}$ mouse was removed from analysis. Data are expressed as mean ± 95% CI except for (**A**).

30

Table 1 Mean network connectivity metrics ± 95% CI in males and females of both genotypes

Age	Adolescence				Adulthood			
C3ar1 status	+/+	-/-	+/+	-/-	+/+	-/-	+/+	-/-
Sex	F	F	M	M	F	F	M	M
Connectivity metric (AUC ± 95% CI)								
FC	25.5 ± 2.0	27.5 ± 3.1	25.9 ± 5.0	29.6 ± 4.5	27.4 ± 3.5	29.3 ± 3.0	30.2 ± 5.7	31.9 ± 4.7
GE	10.3 ± 0.6	11.2 ± 0.8	10.1 ± 0.9	11.3 ± 1.1	10.6 ± 0.8	11.4 ± 0.9	11.4 ± 1.2	12.2 ± 1.3
CC	12.0 ± 0.9	13.0 ± 1.3	12.0 ± 1.9	13.4 ± 1.8	12.8 ± 1.4	13.8 ± 1.4	13.6 ± 2.0	14.4 ± 1.8

FC = functional connectivity, GE = global efficiency, CC = clustering coefficient

Table 2 Mean anxiety-associated node connectivity in males and females of both genotypes

Age	Adolescence				Adulthood			
*C3ar1*status	+/+	-/-	+/+	-/-	+/+	-/-	+/+	-/-
Sex	F	F	M	M	F	F	M	M
Brain area	**Mean node connectivity strength**							
L cingulate cx	0.39	0.41	0.39	0.44	0.45	0.49	0.48	0.54
R cingulate cx	0.38	0.41	0.38	0.43	0.45	0.49	0.48	0.53
L prefrontal cx	0.29	0.33	0.32	0.37	0.41	0.44	0.37	0.49
R prefrontal cx	0.28	0.28	0.33	0.37	0.41	0.45	0.39	0.47
L amygdala	0.14	0.17	0.15	0.2	0.2	0.2	0.24	0.28
R amygdala	0.11	0.16	0.15	0.18	0.19	0.2	0.25	0.25
L pallidum & accumbens	0.23	0.27	0.23	0.31	0.3	0.29	0.35	0.4
R pallidum & accumbens	0.24	0.26	0.24	0.3	0.31	0.31	0.35	0.39
L striatum	0.28	0.32	0.3	0.36	0.32	0.36	0.4	0.43
R striatum	0.26	0.31	0.32	0.35	0.33	0.36	0.42	0.41
L hypothalamus	0.28	0.29	0.27	0.34	0.32	0.32	0.34	0.38
R hypothalamus	0.25	0.27	0.26	0.32	0.31	0.32	0.33	0.37
L dorsal hippocampus	0.4	0.43	0.42	0.49	0.44	0.46	0.48	0.52
R dorsal hippocampus	0.41	0.43	0.42	0.49	0.44	0.47	0.5	0.52
L ventral hippocampus	0.18	0.18	0.17	0.26	0.21	0.23	0.2	0.27
R ventral hippocampus	0.18	0.23	0.19	0.25	0.22	0.25	0.25	0.26
L PAG	0.28	0.3	0.3	0.38	0.27	0.3	0.32	0.36
R PAG	0.28	0.31	0.3	0.39	0.27	0.29	0.32	0.37
L brain stem	0.11	0.11	0.12	0.18	0.1	0.14	0.16	0.16
R brain stem	0.11	0.09	0.12	0.18	0.11	0.13	0.17	0.18

Table 3 Mean behavioural outcome measures ± 95% CI in males and females of both genotypes

Age	Cohort 1				Cohort 2			
C3ar1 status	+/+	-/-	+/+	-/-	+/+	-/-	+/+	-/-
Sex	F		M		F		M	
Anxiety-related	**Untransformed means**							
OF duration core (s)	25.92±12.12	18.74±4.60	19.81±5.35	22.99±7.73	25.06±10.65	29.96±24.36	32.19±18.93	16.71±3.87
OF duration centre (s)	106.94±18.40	102.01±16.36	97.18±13.68	109.40±17.99	105.42±40.78	120.94±39.65	133.80±31.20	95.62±13.10
OF duration periphery (s)	493.13±18.41	498.07±16.36	502.90±13.68	490.66±17.98	493.16±42.58	478.89±39.60	466.11±31.25	504.15±13.10
EPM duration open (s)	29.52±11.52	28.92±12.57	28.06±12.03	28.19±14.72	18.87±8.77	20.45±16.56	15.13±7.96	12.15±7.29
OF latency core (s)	30.66±17.23	44.47±34.34	29.89±16.18	40.95±19.45	34.19±36.91	24.15±20.50	25.86±25.45	29.44±52.19
OF latency centre (s)	10.02±3.52	13.26±8.07	12.35±7.40	11.97±4.95	5.79±6.00	7.45±7.79	5.22±5.01	5.28±4.26
EPM duration middle (s)	109.53±17.89	102.17±19.15	112.33±24.24	122.79±17.27	85.38±21.11	72.59±29.02	71.13±14.54	74.93±17.85
EPM duration closed (s)	176.11±22.18	198.69±19.25	188.78±24.17	178.29±17.22	214.24±21.04	207.31±38.82	227.88±14.86	224.17±17.79
EPM bouts open (#)	4.65±1.92	3.19±1.66	3.44±1.33	2.94±1.18	2.62±1.48	3.43±2.77	2.30±1.12	1.91±1.49
EPM head dips (#)	21.53±6.20	18.12±5.17	19.62±6.29	22.31±5.36	16.75±4.55	17.57±13.16	11.90±3.14	16.73±8.52
EPM stretch-attend postures (#)	19.00±4.15	21.81±2.98	23.62±3.14	23.38±2.87	16.62±6.16	9.43±6.04	13.50±2.68	14.73±4.10
EPM latency open (s)	65.31±27.63	106.76±53.38	92.95±48.81	117.27±51.75	75.66±81.38	83.26±103.55	95.40±71.29	137.52±70.66
Other								
PPI 3 dB (%)					21.11±13.2	15.31±6.40	22.87±7.41	17.14±7.70
PPI 6 dB (%)					40.63±10.16	26.36±8.74	39.49±11.24	34.37±10.65
PPI 12 dB (%)					56.81±13.18	49.81±13.28	57.07±9.51	60.40±8.38
Acoustic startle response at 120 dB (A.U.)					876.35±432.36	1068.32±284.31	1472.99±360.84	1908.79±655.66
NOR recognition index (%)					62.49±11.20	62.60±9.77	65.02±7.66	68.16±8.87
NOR total exploration training (s)					39.45±15.62	38.58±10.66	38.50±12.16	41.12±11.07
NOR total exploration test (s)					31.68±10.07	32.41±6.83	30.81±9.17	33.58±5.39

OF = open field, EPM = elevated plus maze, PPI = prepulse inhibition, NOR = novel object recognition
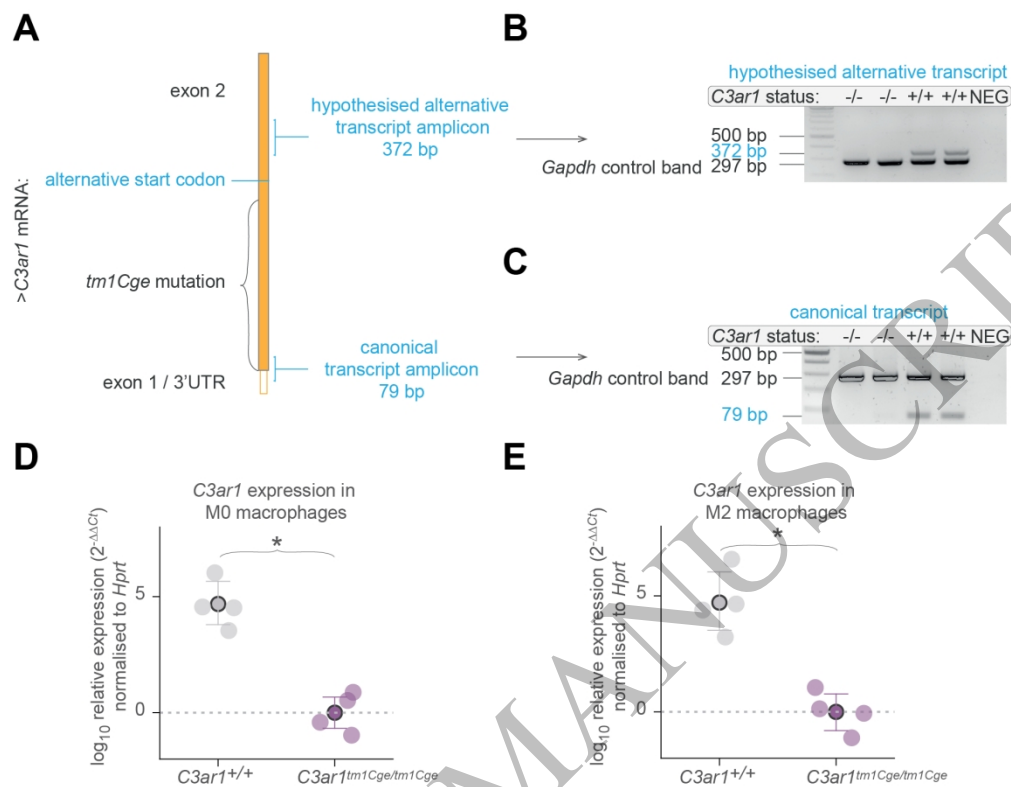
Figure 1 | *C3ar1^{tm1Cge/tm1Cge}* mice lack detectable *C3ar1* mRNA. (**A**) Schematic shows *C3ar1* mRNA with its only protein coding exon and the design of the 79 bp PCR amplicon which targets an exon-1/5' untranslated region (UTR) and exon-2 junction of the canonical *C3ar1* wildtype transcript. Also shown is another 372 bp amplicon which targets a region downstream of the deletion and after an alternative start codon. The start of exon 2 is deleted in *C3ar1^{tm1Cge/tm1Cge}* mice, so PCR should result in no amplification. Similarly, if no alternative transcript is present, there should be no amplification. (**B−C**) Gel images show PCR products of cDNA from bone-marrow derived interleukin 4 (IL4)-induced M2-like macrophages. Each sample well has a 297 bp Glyceraldehyde 3-phosphate dehydrogenase (*Gapdh*) control band. -/- = *C3ar1^{tm1Cge/tm1Cge}*, +/+ = *C3ar1^{+/+}*. NEG: no reverse transcriptase negative control carried over from cDNA synthesis. (**B**) Canonical transcript. (**C**) Hypothesised alternative transcript. The bands appear hollow due to over-saturation. Original uncropped gel images can be found in **Supplemental figure 3**. (**D**, **E**) qPCR of cDNA from bone marrow-derived macrophages: (**D**) M0 and (**E**) M2 from *C3ar1^{tm1Cge/tm1Cge}* mice and wildtype littermates (*N* = 4 mice for each genotype), Kruskal Wallis test M0 $p < 0.05$, M2 $p < 0.05$). Data are presented as mean ± 95% CI. *Hprt* = Hypoxanthine-Guanine Phosphoribosyltransferase 1 (housekeeping gene).
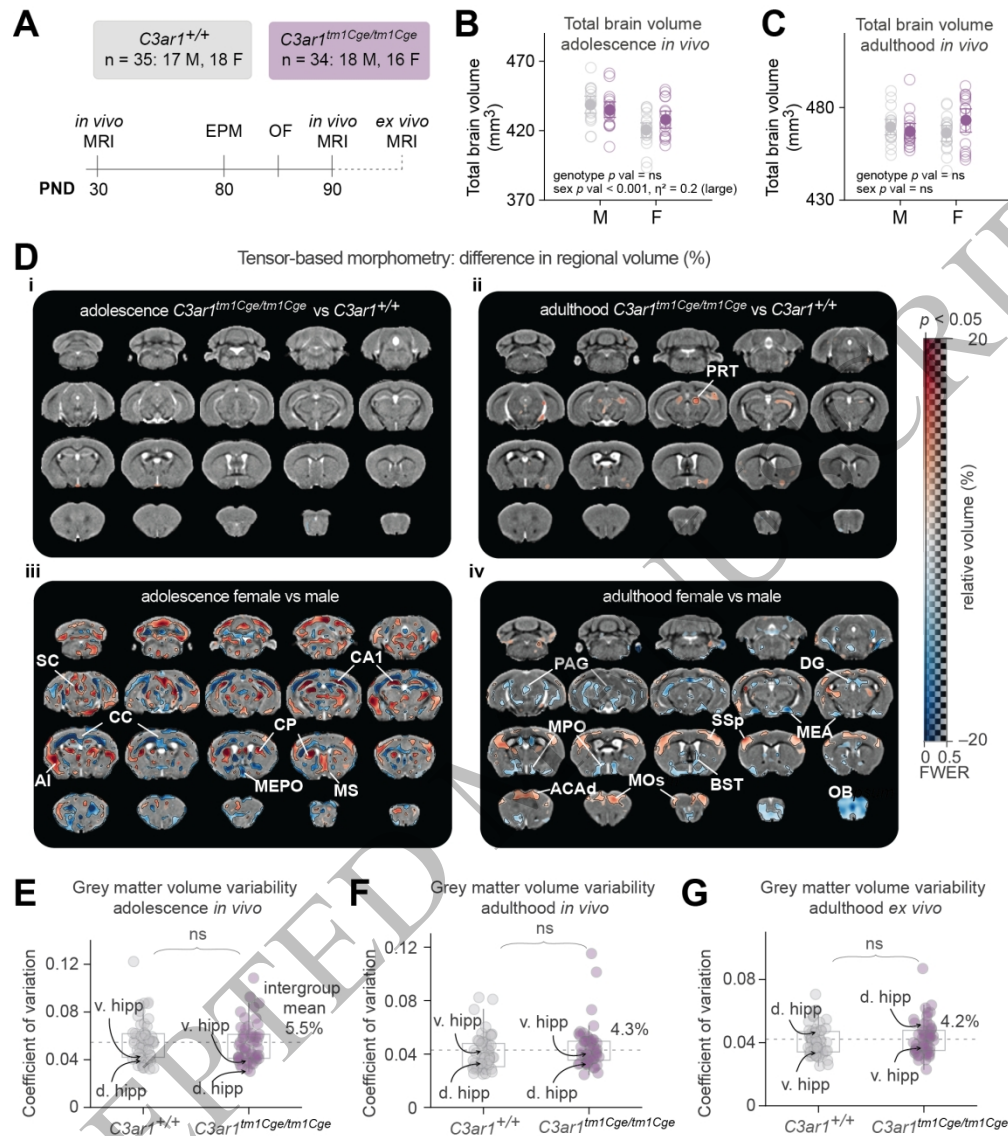
429x334mm (118 x 118 DPI)

Figure 2 | Sex but not *C3ar1* status influences regional brain volume. (**A**) Schematic of the MRI study shown in (**D–G**). 69 mice were scanned twice *in vivo*; in adolescence at ~postnatal day (PND) 30 (range 27-31) and at adulthood ~PND90 (range 81-92), as well as once *ex vivo* after sacrifice after the adulthood scanning session. Behavioural tests were carried out before the adulthood scanning session. EPM = elevated plus maze, OF = open field. (**B**) Total brain volume in adolescence. Two-way ANOVA, genotype, sex, genotype * sex, $F[1,65]$ = 0.35, 16.72, 3.26, p = 0.56, <0.001, 0.76. (**C**) Total brain volume in adulthood. Two-way ANOVA, genotype, sex, genotype * sex, $F[1,65]$ = 0.74, 0.26, 3.33, p = 0.39, 0.61, 0.07. (**B–C**) Data presented as mean ± 95% CI. Each datapoint represents an individual mouse. (**D**) Panels showing relative regional volume changes (%) overlaid on study-specific coronal templates (grey). Red hues signify areas larger in *C3ar1*$^{tm1Cge/tm1Cge}$ (**i–ii**) or females (**iii–iv**) and blue hues signify areas larger in *C3ar1*$^{+/+}$ (**i–ii**) or males (**iii–iv**). Transparency of the colour overlay shows the statistical significance, ranging from family-wise error rate (FWER)-corrected voxel-wise t test p value 0.5 to 0 (transparent to opaque, respectively). Areas where FWE-corrected p value < 0.05 are demarcated with a black line, and where the p value > 0.5 are grey (no overlay), meaning that in adolescence genotype comparison (**i**), no voxels had a p value < 0.5. The locations of the coronal slices in relation to bregma in the left most column

from top: -7.6, -4.6, -1.6, 1.4 mm. *C3ar1$^{+/+}$* *N* = 35, 17 males and 18 females; *C3ar1$^{tm1Cge/tm1Cge}$* *N* = 34, 18 males and 16 females. ACAd = dorsal anterior cingulate cortex, AI = agranular insular cortex, BST = bed nucleus of stria terminalis, CA = cornu ammonis, CP = caudoputamen, DG = dentate gyrus, MEA = medial amygdala, MEPO = medial preoptic nucleus, MOs = secondary motor cortex (MOs), MPO = medial preoptic area, MS = medial septum, OB = olfactory bulb, PAG = periaqueductal grey, PRT = pretectal area, SC = superior colliculus, SSp = primary somatosensory cortex. (**E**) Regional volume coefficient of variation (CV) in adolescence *in vivo*. (**F**) CV in adulthood in vivo. (**G**) CV in adulthood *ex vivo*. (**E–G**) Each data point represents the CV calculated for an individual brain region, using data from all animals; thus, *N* = 66 regions (all atlas regions excluding cerebrospinal fluid areas). Data are shown with quartiles, whiskers show the extent of the distribution. Kruskal Wallis *p* values, all ns. D. hipp = dorsal hippocampus, v. hipp = ventral hippocampus.
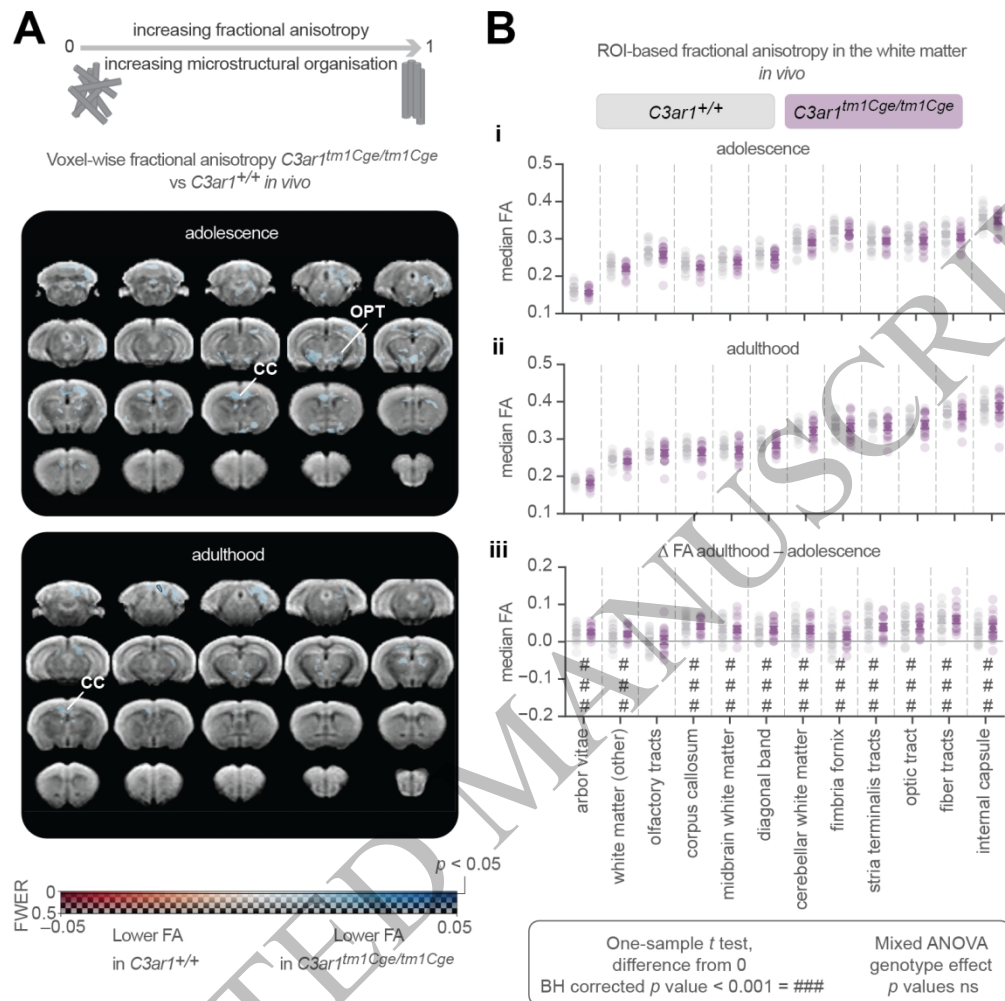
431x489mm (118 x 118 DPI)

Figure 3 | Fractional anisotropy does not depend on *C3ar1* status but increases with age. (**A**) Panels showing voxel-wise fractional anisotropy analysis (voxel-wise *t* tests) in adolescence (top) and adulthood (bottom) corrected for FWER. There are no significant voxels (no black contour) where genotype effect is significant ($p < 0.05$). CC = corpus callosum, OPT = optic tract. (**B**) *In vivo* ROI-based median fractional anisotropy (FA) values in white matter regions for (**i**) adolescence, (**ii**) adulthood and (**iii**) change over time (adulthood − adolescence). Two-sided one-sample *t* test (difference from 0) *p* values that were adjusted with Benjamini-Hochberg (BH) procedure (### *p* value < 0.001). (**Bi−iii**) Mixed ANOVA with genotype and genotype-by-region interaction effects, all ns. Data are presented as mean ± 95% CI. (**A−B**) Adolescence: *C3ar1*$^{+/+}$ *N* = 34, 16 males and 18 females; *C3ar1*$^{tm1Cge/tm1Cge}$ *N* = 33, 17 males and 16 females. Adulthood: *C3ar1*$^{+/+}$ *N* = 31 (15 males and 16 females); *C3ar1*$^{tm1Cge/tm1Cge}$ *N* = 26 (13 males and 13 females). Change: *C3ar1*$^{+/+}$ *N* = 30 (14 males and 16 females); *C3ar1*$^{tm1Cge/tm1Cge}$ *N* = 25 (12 males and 13 females).
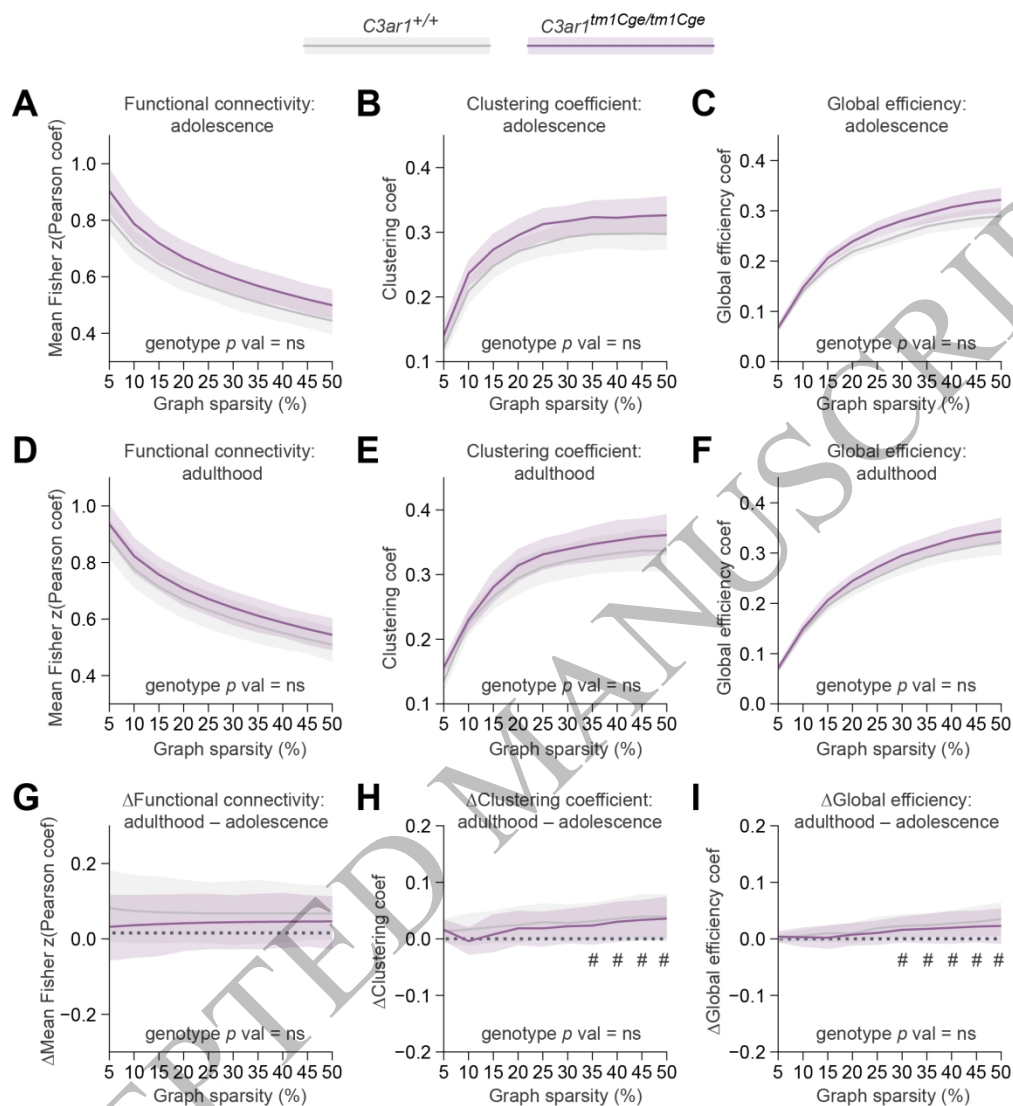
349x350mm (118 x 118 DPI)

Figure 4 | Global functional connectivity is not changed in *C3ar1*|-deficient mice. Functional connectivity, clustering coefficient and global efficiency at decreasing graph sparsity levels in adolescence (**A–C**), and adulthood (**D–F**), and change over time (**G–I**). (**A–I**) Statistical significance was determined with sexes combined using AUC permutation testing (10000 iterations) and the resulting p values were corrected for multiplicity with the Bonferroni method (N = 3 tests per outcome measure). Adolescence: $C3ar1^{+/+}$ N = 32 (15 males, 17 females); $C3ar1^{tm1Cge/tm1Cge}$ N = 32 (18 males, 14 females); Adulthood: $C3ar1^{+/+}$ N = 33 (16 males, 17 females) and $C3ar1^{tm1Cge/tm1Cge}$ N = 32 (17 males, 15 females); change: $C3ar1^{+/+}$ N = 30 (14 males and 16 females); $C3ar1^{tm1Cge/tm1Cge}$ N = 31 (17 males and 14 females). Data are shown as mean ± 95% CI. (**G–I**) Two-sided one-sample t tests (difference from 0) for global connectivity changes at each sparsity level with genotypes combined, corrected using the BH procedure (N = 10 sparsity levels), # = adjusted p value < 0.05. Coef = coefficient.
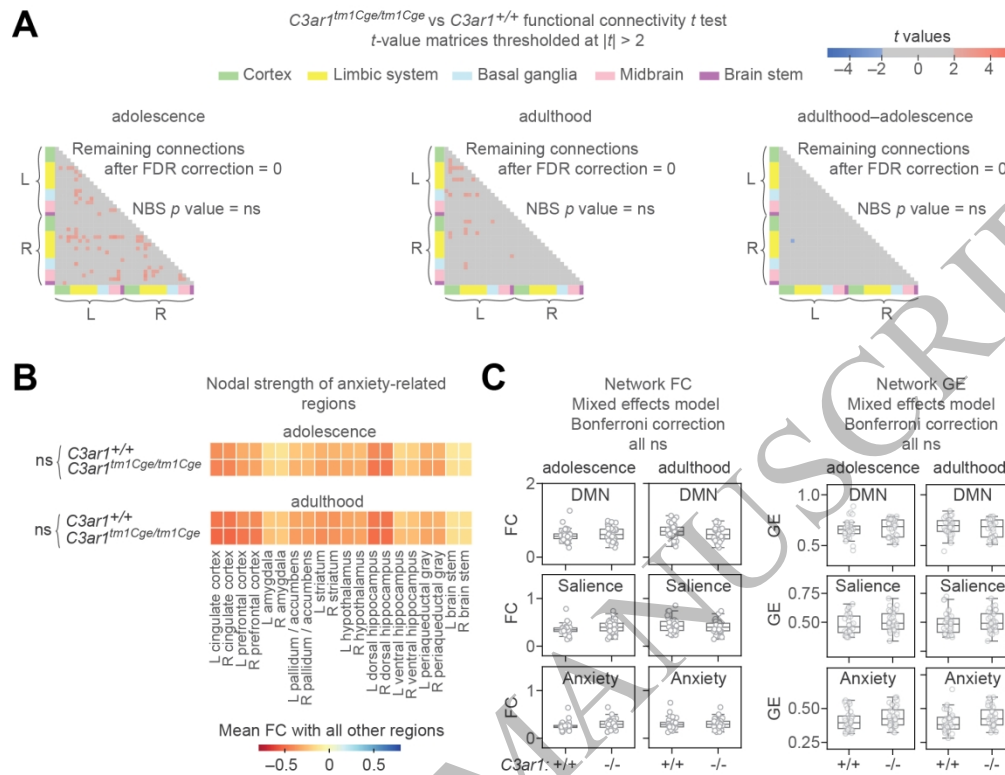
432x474mm (118 x 118 DPI)

Figure 5 | *C3ar1*-deficiency does not influence functional brain networks. (**A**) Thresholded adjacency matrices comparing *C3ar1*$^{+/+}$ and *C3ar1*$^{tm1Cge/tm1Cge}$ mice where $|t| \geq 2$ in adolescence and adulthood, and the change between time points. No connections with $|t| \geq 2$ remained significant after the false discovery rate (FDR) correction. Additionally, the number of connections in the $|t| \geq 2$ adjacency matrix components were not significant when assessed using network-based statistics (NBS) correction. (**B**) Nodal strength (mean absolute connectivity) of a priori anxiety-related seeds (e.g. L cingulate cortex correlation coefficients with all other regions). *P* values were calculated using a mixed ANOVA with between-subjects factor of genotype and within-subjects factor of region. Only the region effect was significant at both time-points (both *p* values < 0.001, $\eta_p^2 = 0.69$ in adolescence and $\eta_p^2 = 0.73$ in adulthood). (**C**) Functional connectivity (FC) and global efficiency (GE) were analysed using mixed effects linear models with genotype, time point (adolescence and adulthood) and their interaction as fixed effects and mouse ID as a random effect. Analyses were run separately for each network, corrected with the Bonferroni method (three tests). All *p* values = ns. (**A–C**) Adolescence: *C3ar1*$^{+/+}$ *N* = 32 (15 males, 17 females); *C3ar1*$^{tm1Cge/tm1Cge}$ *N* = 32 (18 males, 14 females); Adulthood: *C3ar1*$^{+/+}$ *N* = 33 (16 males, 17 females) and *C3ar1*$^{tm1Cge/tm1Cge}$ *N* = 32 (17 males, 15 females).
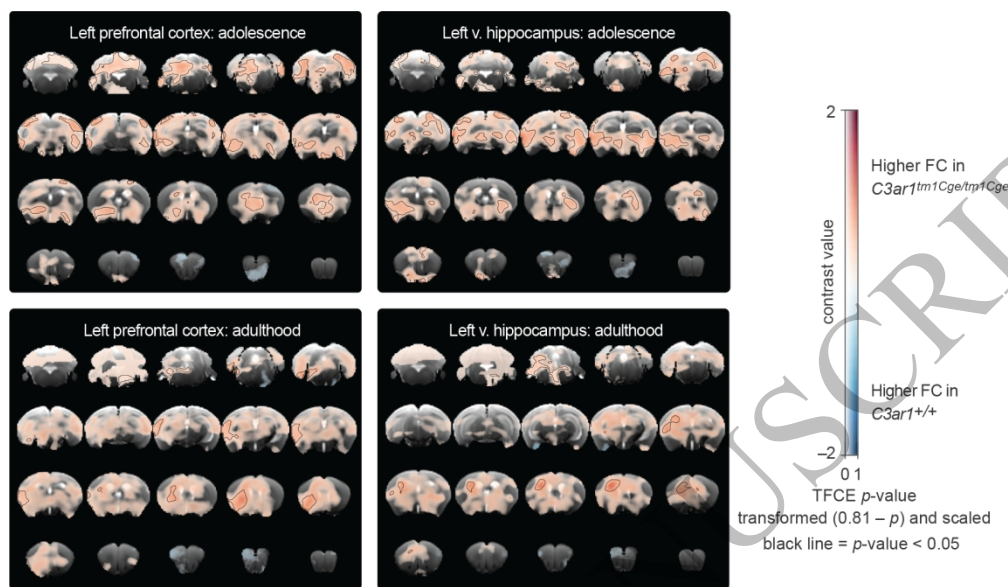
431x332mm (118 x 118 DPI)

Figure 6 | Examples of seed-based FC maps. Shown are voxel-wise group differences between $C3ar1^{tm1Cge/tm1Cge}$ and $C3ar1^{+/+}$ mice (using t tests) with seeds placed in the left ventral hippocampus and left prefrontal cortex in adolescence and adulthood datasets. The dual scale bar displays contrast value on the x-axis and TFCE p-values (transformed $0.81 - p$) on the y-axis. The transformed p-values have been re-scaled to range from 0 to 1 for visualisation, with darker colours representing greater statistical significance. Black outlines demarcate regions where TFCE p-values are below 0.05. Adolescence: $C3ar1^{+/+}$ $N = 32$ (15 males, 17 females); $C3ar1^{tm1Cge/tm1Cge}$ $N = 32$ (18 males, 14 females); Adulthood: $C3ar1^{+/+}$ $N = 33$ (16 males, 17 females) and $C3ar1^{tm1Cge/tm1Cge}$ $N = 32$ (17 males, 15 females).
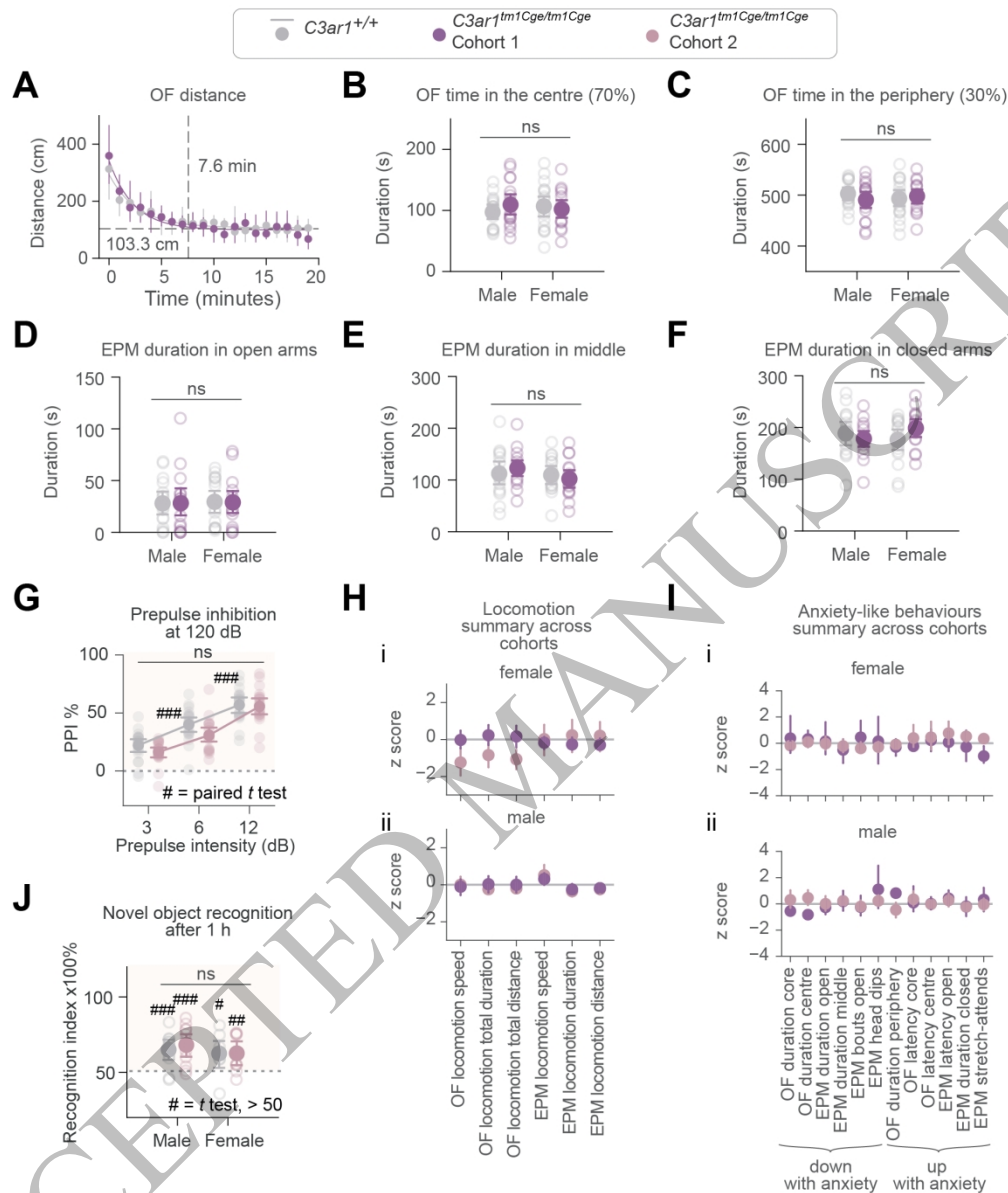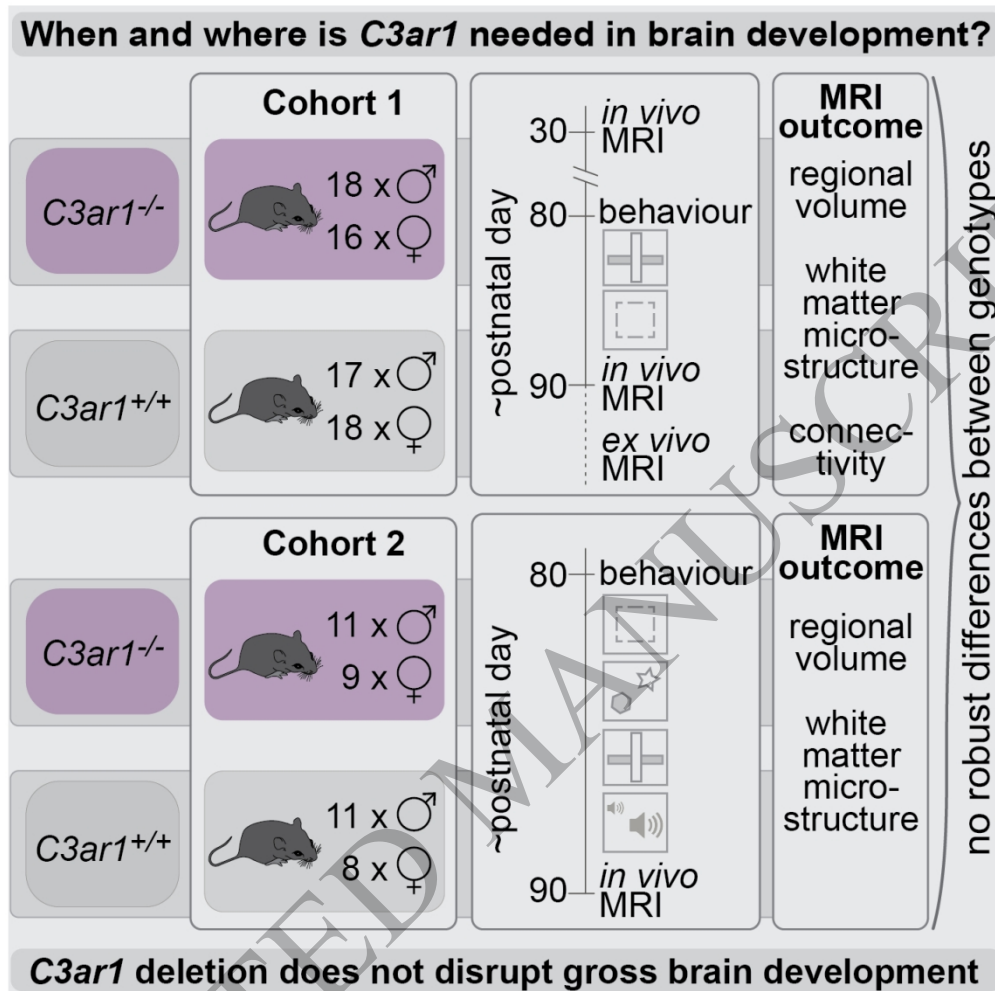
425x266mm (118 x 118 DPI)

Figure 7 | *C3ar1* deficiency does not cause behavioural abnormalities. (**A**) Cohort 1 OF distance travelled in one-minute bins plotted as median ± interquartile range, fitted with exponential decay curves; dotted lines show the asymptote and the time animals reach 95% stability in distance travelled per minute. Effects of time bin, genotype and their interaction tested with two-way ANOVA; only time was significant ($p < 0.01$). (**B–F**) Cohort 1 OF and EPM: anxiety-like outcomes for $C3ar1^{+/+}$ and $C3ar1^{tm1Cge/tm1Cge}$ mice, separated by sex. Statistical comparisons made using two-way ANOVA (genotype × sex) for each metric; all effects ns so no post-hoc comparisons were performed. Individual p values can be found in **Supplemental table 5**. (**G**) Prepulse inhibition (PPI) in Cohort 2. Individuals plotted per genotype, and sexes are separated only for visualisation. PPI increased with increasing prepulse intensity in both genotypes (paired t tests p value ### < 0.001); no genotype differences by Student's t tests ($C3ar1^{+/+}$ vs $C3ar1^{tm1Cge/tm1Cge}$ all p values > 0.05). Dashed line marks inhibition threshold.(**H–I**) Z-scored locomotion and anxiety metrics for $C3ar1^{tm1Cge/tm1Cge}$ mice normalised to $C3ar1^{+/+}$ mean, showing Cohorts 1 and 2. (**J**) Novel object recognition recall 1 h after acquisition in Cohort 2. Sexes are separated only for visualisation. Both

genotypes showed novelty preference (one-sample t test, value > 50/chance, # = $p < 0.05$, ## = $p < 0.01$ ### = $p < 0.001$). There were no differences between groups ($C3ar1^{+/+}$ vs $C3ar1^{tm1Cge/tm1Cge}$ Student's t test $t[37] = 0.42$, $p = 0.67$). (**A–I**). Experimental units are individual mice. Cohort 1: $C3ar1^{tm1Cge/tm1Cge}$ N = 34 (18 male, 16 female), $C3ar1^{+/+}$ N = 35 (17 male, 18 female), except for EPM where one $C3ar1^{tm1Cge/tm1Cge}$ mouse (male) and two $C3ar1^{+/+}$ mice (one male, one female) were removed from analysis due to falling off the open arm. Cohort 2: $C3ar1^{tm1Cge/tm1Cge}$ N = 20, $C3ar1^{+/+}$ N = 19 (males and females combined), except for EPM where two female $C3ar1^{tm1Cge/tm1Cge}$ mice and one male $C3ar1^{+/+}$ mouse was removed from analysis. Data are expressed as mean ± 95% CI except for (**A**).

432x514mm (118 x 118 DPI)

Graphical abstract

307x306mm (118 x 118 DPI)